Thesis Report

submitted within the UNIGIS MSc. programme
at the Department of Geoinformatics - Z_GIS
University of Salzburg, Austria
under the provisions of UNIGIS framework

Comparative Study of Landslide Susceptibility Analysis by using different techniques along the Pasang Lhamu Highway

by

Sujan Khatiwada
U105623

A thesis submitted in partial fulfilment of the requirements of
the degree of
Master of Science (Geographical Information Science & Systems) – MSc (GISc)

Advisor: Dr. Him Lal Shrestha

Kathmandu, 03.10.2023

Science Pledge

By my signature below, I certify that my thesis report is entirely the result of my own work. I have cited all sources of information and data I have used in my thesis report and indicated their origin.

Kathmandu, 03.10.2023 *Sujan.*

Place and Date	Signature

Acknowledgements

It's my pleasure to acknowledge the contribution and support of various persons and organizations to complete this study. I want to thank the Department of Geoinformatics - Z_GIS University of Salzburg for giving me the chance to complete this project work I would like to sincerely thank my supervisor, Dr. Him Lal Shrestha, for his direction, encouragement, and support throughout my research endeavor. His insightful comments and suggestions have been instrumental in shaping my research direction and improving the quality of my work. Also, I would like to thank Dr. Upama Koju and Dr. Ambika P. Gautam for providing their valuable feedback to complete this thesis work. Also, I would like to express my thanks to whole Kathmandu Forestry College Family for directly and indirectly helping me completing of the project work I would like to thank everyone at Kathmandu Forestry College for their direct and indirect assistance in helping me finish the project work

My special thanks go towards my brother Nirdosh Khatiwada and Er. Anil Gajurel for his support in field study period. I am equally thankful to all teaching faculties and staff members of Kathmandu Forestry College. I am grateful to my family for their unwavering love and support, especially during the challenging times of this research work. Lastly, I would like to thank all the participants who took part in my research project. Without their valuable contributions, this study would not have been possible.

Abstract

In steep and mountainous terrains, landslides are one of the most obviously devastating events. The Pasang Lhamu Highway, which connects Kathmandu to Dhunche via Nuwakot, receives a high volume of landslides every year during monsoon season, causing recurring issues for pilgrims and local citizens. For the current study, six kilometers buffer of the Pasang Lhamu Highway, extending from Kathmandu to Dhunche, was chosen for Landslide Susceptibility Assessment, applying Analytical Hierarchy Process (AHP) and Frequency Ratio (FR) methods. Ten factors causing landslides were selected, and a Landslide Susceptibility Maps were created. Landslide inventory was conducted by visiting sites and utilizing high-resolution satellite images. A total of 218 landslide events were recorded and randomly split into training landslides (70%) and testing landslides (30%) datasets. The frequency of landslide events and the landslide area in each factor's classes were examined, and the relationship between landslides and causative factors' classes was statistically evaluated using FR and weighted value. Finally, Landslide Susceptibility Index (LSI) maps were prepared. According to the FR model, high and very high susceptibility classes account for 14.04% and 6.29%, respectively, of the research region, while it is 21.02% and 12.56% from the AHP model. Similarly, according to the FR model, 9.58 and 11.83 square kilometers of forest and cropland are located in the very high susceptibility class, respectively, while it is 30.70 and 23.21 square kilometers as per the AHP model. The final LSI maps were validated using the Area Under a Curve (AUC) method. From FR model, AUC for success rate, and prediction rate were found to be 86.29% and 84.96%, respectively, while it was 82.93% and 75.28%, respectively, in the AHP model. This study indicates that the FR model is better suited for predicting future landslides than the AHP model.

Key Words: *Analytical Hierarchy Process, Frequency Ratio, Landslides, Causative Factors and Susceptibility.*

Abbreviations and Acronyms

AHP	Analytical Hierarchy Process
ANN	Artificial Neural Network
AUC	Area Under a Curve
CI	Consistency Index
CR	Consistency Ratio
DEM	Digital Elevation Model
ESRI	Environmental System Research Institute
FR	Frequency Ratio
GIS	Geographic Information System
ICIMOD	International Centre for Integrated Mountain Development
Km	Kilometer
LSI	Landslide Susceptibility Index
LSM	Landslide Susceptibility Mapping
LULC	Land Use Land Cover
m	Meter
MCDA	Multi-Criteria Decision Analysis
mm	Millimeter
MoHA	Ministry of Home Affairs
NH	National Highway
PGA	Peak Ground Acceleration
ROC	Receiver Operating Characteristics
RS	Remote Sensing
SNAP	Sentinel Application Platform
TWI	Topographic Wetness Index
UTM	Universal Transverse Mercator
WGS	World Geodetic System

Table of Contents

Contents

Science Pledge ..... **I**

Acknowledgements ..... **II**

Abstract ..... **III**

Abbreviations and Acronyms ..... **IV**

Table of Contents ..... **V**

List of Tables ..... **VIII**

List of Figures ..... **VIII**

List of Maps ..... **VIII**

Chapter-1: Introduction **1**

1.1 Background 1

1.2 Problem Statement and justification 2

1.3 Research questions 3

1.4 Objectives 4

1.4.1 General objective 4

1.4.2 Specific Objectives 4

Chapter-2: Literature Review **5**

Chapter-3: Materials and Methods 8

3.1 Study Area..... 8
3.1.1 Description 9
3.1.2 Geological settings 9

3.2 Data types 10
3.2.1 Landslide Point and Polygon Data 10
3.2.2 Sentine-2 image 11
3.2.3 ALOS PALSAR Dem and its derivatives 11
3.2.4 Road networks..... 11
3.2.5 Climatic Data 12
3.2.6 Geology 12

3.3 Software used..... 13

3.4 Methodological flow chart of study 13

3.5 Selection of landslide causative factors and data preparation 15
3.5.1 Slope 15
3.5.2 Aspect of slope 16
3.5.3 Elevation..... 16
3.5.4 Curvature profile 17
3.5.5 Geology (Lithology) 17
3.5.6 Land use land cover 18
3.5.7 Distance to road networks 19
3.5.8 Distance to drainage networks..... 20
3.5.9 Precipitation..... 20
3.5.10 Topographic Wetness Index (TWI)..... 21

3.6 Image Pre-processing..... 22
3.6.1 Compositing and Mosaicking Bands 22

3.7 Data Processing 22
3.7.1 Clipping 22
3.7.2 Rasterization 22
3.7.3 Resampling 22
3.7.4 Size of grid 23
3.7.5 Coordinate System Projection 23

3.8 Landslides Inventories and Mapping..... 23

3.9 Landslide Susceptibility Mapping 24
3.9.1 Analytical Hierarchy Process 24
3.9.1.1 Weighting value for factor/factor's classes..... 24
3.9.1.2 Landslide Susceptibility Index from AHP method 27

3.10 Frequency Ratio method 28
3.10.1 Landslide Susceptibility Index from Frequency Ratio method 28

3.11 Assessment of LULC in different Susceptibility Classes 29

3.12 Validation of Landslide susceptibility Map 29

Chapter-4: Results 31

4.1 Landslide Inventory 31

..... 32

4.2 Landslide causative factors 32
4.2.1 Slope 32
4.2.2 Aspect 34
4.2.3 Curvature profile 35
..... 36
4.2.4 Elevation 37
..... 38
4.2.5 Topographic Wetness Index 38
4.2.6 Precipitation 39
..... 41
4.2.7 Land Use Land Cover 41
4.2.8 Geology 43
4.2.9 Distance to drainage 44
..... 46
4.2.10 Distance to road networks 46

4.3 Landslide Susceptibility Mapping 47
4.3.1 Frequency Ratio Model 47
4.3.1.1 Landslide Susceptibility Index map from FR 51
4.3.2 AHP model 52
4.3.2.1 Landslide Susceptibility Map from AHP method 57

4.4 Validation of Landslide Susceptibility Map 58

4.5 Land Use Land Cover in different Susceptibility Classes 60
4.5.1 LULC in Frequency Ratio Model 60
4.5.2 LULC in Analytical Hierarchy Process Model 60

4.6 Comparison of LSI maps 60
4.6.1 Susceptibility Class, training landslides and testing landslide areas 60
4.6.2 Area coverage by LULC in different susceptibility class 62
4.6.3 Accuracy assessment of Models 62

Chapter-5: Discussions **64**

Chapter-6: Conclusion **69**

Chater-7: Reference **71**

List of Tables

Table 1: Summary of datasets used in research 12
Table 2: Random consistency Index (Saaty, 1980) 27
Table 3: Preference and Judgement Scale (Saaty, 1980) 27
Table 4: Landslides in different slope classes 33
Table 5: Landslides in different classes of aspect 34
Table 6: Landslides in different classes of curvature classes 36
Table 7: Landslides in different elevation class 38
Table 8: Landslides in different TWI classes 38
Table 9: Landslide in different precipitation classes 41
Table 10: Landslide in different classes of LULC 41
Table 11: Error matrix: accuracy assessment for Supervise classification of LULC classes 43
Table 12: Landslides in different geological formation class 43
Table 13: Landslide at different distance from drainage networks 46
Table 14: Landslide at different distance from road network 46
Table 15: Frequency ratio of causative factors 48
Table 16: The pair-wise comparison matrix, factor weights and consistency ratio 53
Table 17: The pair-wise comparison matrix, class weights (rating) and consistency ratio 53
Table 18: Area of LULC located in different susceptibility class of LSI map prepared from FR method (Area in square kilometer) 60
Table 19: Area of LULC located in different susceptibility class of LSI map prepared from AHP method (Area in square kilometer) 60
Table 20; Comparison table for map obtained from FR and AHP Model 61

List of Figures

Figure 1: Methodological flow chart of the study 14
Figure 2: Supervised Classification steps 18
Figure 3: Success rate curve rate for Frequency Ratio Model 59
Figure 4: Success rate and prediction rate for AHP model 59
Figure 5: Area coverage by LULC in different susceptibility classes 62

List of Maps

Map 1: Map of study area 8
Map 2: Landslide point datasets of study area 31

Map 3: Landslide polygon datasets of study area 32
Map 4: Slope of the study area 33
Map 5: Aspect map of the study area 35
Map 6: Curvature profile of study area 36
Map 7: Elevation Map of area 37
Map 8: TWI map of the study area 39
Map 9: Precipitation map of study area 40
Map 10: Land Use Land Cover of study area 42
Map 11: Geology of study area 44
Map 12: Euclidean distance of drainage network 45
Map 13: Euclidean distance of road networks 47
Map 14: Landslide Susceptibility map from Frequency Ratio Method 52
Map 15: Landslide Susceptibility Index Map from AHP Method 58

Chapter-1: Introduction

1.1 Background

A disaster refers to a sudden and catastrophic occurrence that severely disturbs the normal operations of a society or community, causing losses in terms of human life, property, economy, or the environment beyond the capacity of the community or society to manage independently (Joseph et al., 2016). One of the natural calamities that present a significant risk for human casualties and property damage is landslides (Dai et al., 2002). During the monsoon season, floods and landslides occur frequently, resulting in massive losses of life and property. MoHA (2017) estimated that landslides alone caused economic losses of around $8.11 million in the 2015-2016 year, affecting more than 5.94 million people in Nepal. The risk of landslides is strongly correlated with development activities and increases with urbanization, development activities, ongoing deforestation in the areas prone to landslide, higher precipitation, and seismic activity (Pathak, 2016). Anthropogenic activities like improper land use practices, haphazard irrigation canal construction without adequate safety precautions in sensitive mountain regions, and uncontrolled development projects like road toe cutting in Nepal all raise the danger of landslides (Petley et al., 2007). Highway construction and road expansion along mountain areas, in particular, increases the probability of landslide occurrence (Glade, 2003).

To manage landslides systematically, landslide evaluation and susceptibility zonation are necessary. Over the past ten years, a number of techniques for landslide appraisal and zonation have been created (Shano et al., 2020). A semi-quantitative method widely used for Landslide Susceptibility Analysis is multi-criteria decision analysis (MCDA) approaches (Erener et al., 2016). Statistical models have recently been employed by academics to produce maps of landslide susceptibility, and some of these models integrate with other methods including Analytical Hierarchy Process (AHP) and Frequency Ratio (FR) methodologies (Demir et al., 2012). The AHP, created by Saaty (1980), is a Multi-Criteria

Decision-Making approach that employs pairwise comparisons to measure priority scales and is reliant on expert judgments (Saaty, 2008). Thapa and Bhandari (2019) employed the Frequency Ratio approach to pinpoint potentially landslide-susceptible regions in the Siwalik region of the Chatara-Barahakshetra segment. Yalcin et al. (2011) explains that the Frequency Ratio (FR) is a statistical method for evaluating landslide susceptibility that takes into account the relationship between the occurrence of landslides and the underlying factors causing them. In order to determine the susceptibility to landslides, Veerappan et al. (2017) conducted a comparison study between the FR and the AHP method on a section of the National Highway (NH-58) in Uttarakhand, India. According to Panchal & Shrivastava's (2021) comparative study among FR, AHP, and Shannons Entropy, FR is the best model for assessing the Landslide Susceptibility of Shimla district of Himachal Pradesh.

1.2 Problem Statement and justification

The study area, Pasang Lhamu highway is one of the important Highway of Nepal which is extended from Kathmandu to Dhunche. This Highway receives high traffic volumes and is important for exporting and importing goods between China and Nepal. According to Acharya et al. (2005) rugged topography, complex geological structure and extreme rainfall are the natural causes of landslide. Highway widening is also going on from Tinpiple (Kathmandu) to Tadi (Nuwakot) of the Highway which might be the additional inducing driving factor for slope instability. Unplanned/unscientific urbanization or development of built-up area in the hilly slope (Lai et al., 2013), road construction activities, improper land use practice and deforestations are the additional enhancing factors which further contribute for more landslide and soil erosion. Every year during the monsoon season, this Highway and its associated areas are frequently blocked by landslides, which causes human casualties, cattle losses, and societal and individual property losses.

Landslide Susceptibility Assessment is a very complicated process and is frequently relies on index, statistical relationship or physical process. In countries like Nepal landslides related studies are only conducted to record the effects in the impacted areas after landslide accidents. However, there has been a significant increase in landslide studies and prediction in recent years (Kayastha et al., 2013; Acharya and Lee 2018; Pradhan et al., 2010). Yet, there hasn't been enough research done to determine the magnitude of past damage and anticipate probable damage in future. The occurrence of landslides has a tendency to be concentrated in areas where they have previously taken place, so a thorough understanding of their spatial distributions is necessary to reduce the effects they have on human life and property (Thapa & Bhandari, 2019). Landslide susceptibility analysis is an important approach for identifying areas that are prone to landslides, but there are still numerous challenges that need to be overcome. The quality and availability of the data, as well as the methodologies used for analysis, have a significant impact on the accuracy and reliability of landslide susceptibility mapping. So, for the detail understanding of the correlation between landslides and its causative factors as well as developing LSI map for categorizing the study area in into different landslide susceptibility zone, comparative study between FR and AHP was conducted considering ten causative factors.

Landslide susceptibility assessment can help identify areas at risk of landslides, enabling stakeholders to take necessary measures to mitigate the risks. This could include measures such as slope stabilization, vegetation management, or implementing early warning systems. Understanding landslide susceptibility can help authorities to be prepared for emergency response in the case of landslide incidents. This includes evacuation planning, search and rescue, and other measures to ensure public safety.

1.3 Research questions

- How the landslide events are distributed in the study area?
- Which landslide causative factor's class is highly contributing to landslide

occurrence?

- How much areas are covered by different susceptibility classes?
- Which method gives better result for Landslide Susceptibility Assessment?
- How much areas of Land Use Land Cover are located in different level of susceptibility classes?

1.4 Objectives

1.4.1 General objective

- To carryout Landslide Susceptibility Analysis along Pasang Lhamu Highway by using Frequency Ratio and Analytical Hierarchy Process Methods.

1.4.2 Specific Objectives

The specific objectives of the study area are:

- To map landslide events and develop landslide inventory map,
- To assess the contribution of factors' classes to landslide occurrence based on frequency, frequency ratio and landslide area,
- To assess the area in different susceptibility classes,
- To compare the Landslide Susceptibility of study area derived from Analytical Hierarchy Process and Frequency Ratio methods and
- To assess the land cover in different level of susceptibility classes

Chapter-2: Literature Review

In steep areas, landslides are the most harmful geological hazard (Shano et al., 2020). Nepal has a fragile environment, and frequent landslides are due to physiographic and topographic conditions (Adhikari and Koshimizu, 2005), high seismicity (Khanal and Watanabe, 2008), and highly concentrated rainfall during the monsoon season. Moreover, anthropogenic factors like unplanned/unscientific urbanization, development of built-up areas on hilly slopes (Lai et al., 2013), inadequate land use practices, deforestation, and road construction are further aggravating variables that increase the likelihood of landslides and soil erosion. Highway construction and road expansion along mountain regions, in particular, increase the chance of landslide occurrence (Glade, 2003). Compared to other land uses, roads contribute the most to surface erosion and landslide losses (Sidle et al., 2006). Specifically in developing countries, landslides near highways are highly vulnerable due to often poor engineering design (Sidle et al., 2006). Landslides induced by rainfall are frequent along the road corridor, which is more disastrous (Timilsina & Dahal, 2013).

In order to manage and lessen the impact of landslides, it is essential to undertake hazard zonation and landslide appraisal (Shano et al., 2020). There are various techniques available for assessing landslide risk, and choosing the most effective one is crucial (Shano et al., 2020). A number of land-related factors are required for landslide susceptibility mapping and analysis. Landslides can be recognized, evaluated, monitored, and managed by using Geographic Information Systems (GIS) and Remote Sensing (RS) in combination with other datasets. GIS provides powerful spatial analytic capabilities to extract and evaluate important information, enabling scientific decision-making. RS, on the other hand, facilitates immediate topography surveying and landslide event monitoring (Pradhan et al., 2010).

Researchers all across the world have generated landslide inventory using GIS and RS, as well as maps of susceptibility at local and regional scales (Guzzetti et al., 2012; Xu, 2015; Yang et al., 2016; Pokharel and Thapa, 2019). AHP, a semi-quantitative technique founded on prioritization through deconstruction, comparative assessment, and synthesis, has been identified by Saaty (1980) and Yalcin and Bulut (2006) as commonly useful for regional susceptibility assessments. Saaty (1980) introduced AHP as an MCDA approach to simplify complex decisions for subjective evaluation (Tyagi et al., 2022). By contrasting them pair-wise, it enables decision-makers to gauge the relative relevance of various factors (Yoon and Hwang, 1995). The AHP's ability to assess the consistency of weights is a desirable characteristic. The eigenvalues produced by the calculation determine the matrix's consistency, which is established by Saaty (1980). The AHP technique can uncover and fix any inconsistencies discovered during the decision-making process. As a result, the AHP approach is frequently superior to alternative models for LSM (Tyagi et al., 2022). Although assigning relative weightage values to landslide-causing factors by an individual is often difficult for others to comprehend, according to Kumar and Anbalagan (2016), if weights are based on previous landslide data, they can be more easily understood (Tyagi et al., 2022). The FR model has also emerged as a popular and practical quantitative method for landslide susceptibility mapping. This method is based on past landslide events and their geographical extent (Mondal & Maiti, 2013). Lee and Pradhan (2006) claim that the FR model makes a connection between past landslide locations and the many contributing factors that need to be considered.

El Jazouli et al. (2019) applied the AHP model to map landslide susceptibility by considering land-related parameters such as land cover, lithology, distance to roads, faults, drainage networks, elevation, aspect, and slope gradient. Reis et al. (2011) integrated FR with the AHP method, while Park et al. (2012) proposed a Landslide Susceptibility Index Map by combining AHP, FR, an Artificial Neural Network (ANN) and Logistic Regression methods. The comparative study conducted by Panchal &

Shrivastava (2021) among FR, AHP, and Shannon's Entropy revealed that FR is the suitable model for assessing the landslide susceptibility of the Shimla district of Himachal Pradesh. Research conducted by Veerappan et al. (2017) on part of National Highway (NH-58), Uttarakhand, also shown the similar result. However, the research of Asmare (2023) conducted in Choke Mountain, northwestern Ethiopia, showed that AHP is the finest method compared to FR as AHP had more accuracy. Asmare (2023), Veerappan et al. (2017) and Panchal & Shrivastava (2021) evaluated the accuracy of the LSI map by using ROC curves. The AUC of the success rate demonstrates the capability of landslide techniques to accurately categorize the occurrence of existing landslides, while the AUC of the prediction rate represents the capability of the suggested landslide method to anticipate landslide susceptibility (Asmare, 2023). For statistical, artificial intelligence, and semi-quantitative approaches like fuzzy logic, AHP, etc., statistical validations are used, while all statistical techniques, machine learning, artificial intelligence, and some semi-quantitative approaches are commonly evaluated using field observations and statistical tests (Shano et al., 2020). With the exception of small area or single landslide studies, sample field observations may be applicable to all landslide studies. Shano et al. (2020) state that the ROC curve is the predominant method used to evaluate the predictive abilities of the methodologies mentioned above. It involves plotting the probability of correctly identifying landslides against the probability of falsely identifying landslides as the cut-off probability is varied.

Chapter-3: Materials and Methods

3.1 Study Area

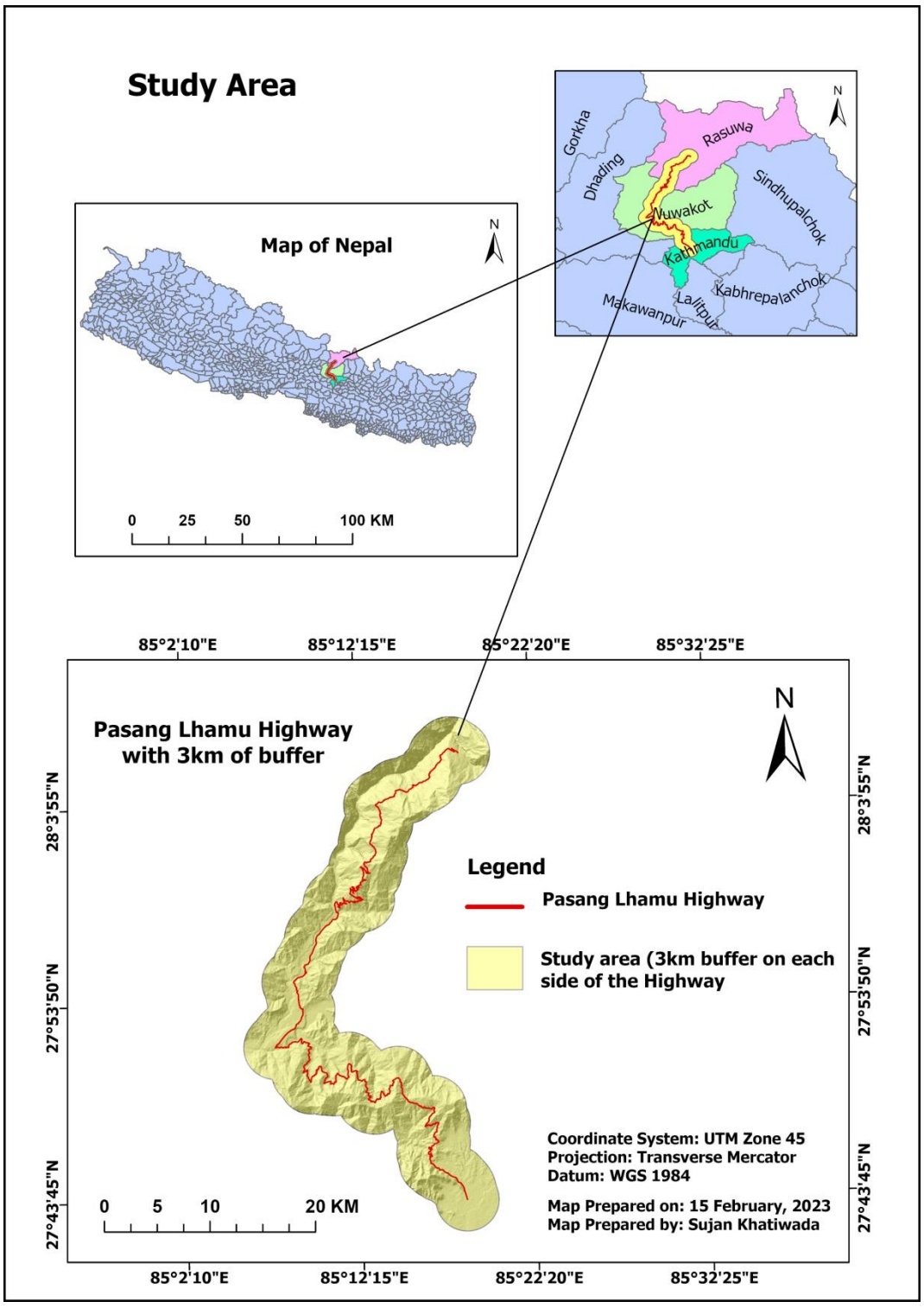

Map 1: Map of study area

3.1.1 Description

Pasang Lhamu highyway is one of the important Highway of Nepal which is extended from Kathmandu to Dhunche. It touches three districts of Nepal: Kathmandu, Nuwakot and Rasuwa. The research was conducted within 6 km buffer zone from the Highway. The study area is extended from 85°18’16”°E and 27°42’01”N (Kathmandu) to 85°18’16”E and 28°8’25”N (Dhunche). The research area covers about 441 km², while the length of the road considered in the study is approximately 114 km. Trishuli and Tadi are the two major rivers. Although the study area mainly covers three districts, Nuwakot and Rasuwa are recorded to have high landslide events. According to the Central Bureau of Statistics, Nepal (2021), the estimated population of Nuwakot district as of 2021 is 2,62,981 while that of Rasuwa is 45,554. The study area covers 51.28% of forest land followed by 37.62% of cropland and 7.94% of built-up areas (Table 10). The study area ranges from the lower altitude with 408 meters to the maximum altitude to 3611 meters with a slope range from 0º To 79º. Kakani, which is located at an altitude of 1729.14 meters above sea level, has a subarctic climate with chilly summers and dry winters. The annual temperature in the district is 19.08º C, which is -2.92% lower than Nepal's averages. Kakani of Nuwakot typically receives about 349.2 millimeters of precipitation and has 207.37 rainy days annually (TckTckTck, n.d.). Similarly, Situated at an elevation of 2148.28 meters from the sea level, the subarctic climate of Dhunche features chilly summers and dry winters. The district's annual temperature is 20.39º C, which is -1.61% lower than Nepal's average. Dhunche, headquarter of Rasuwa, typically experiences 221.52 rainy days with precipitation of 373.03 millimeters annually Weather and Climate (TckTckTck, n.d.).

3.1.2 Geological settings

Nepal has been classified into five major tectonic zones based on its geological and tectonic features, namely the Terai Zone, Siwalik Zone, Lesser Himalayan Zone, Higher Himalayan Zone, and Tibetan-Tethys Himalayan Zone (Ganser, 1964). These zones are

separated by four distinct boundaries: the Main Frontal Thrust (MFT), Main Boundary Thrust (MBT), Main Central Thrust (MCT), and South Tibetan Detachment System (STDS), which demarcate the Terai and Siwalik Zone, Siwalik and Lesser Himalayan Zone, Lesser Himalayan Zone and Higher Himalayan Zone, and Higher Himalayan and Tibetan-Tethys Himalayan Zones (Dahal, 2013). The Lesser Himalayan Zone makes up the majority of the research area, while the Higher Himalayan Zone makes up some of it. With a minor association of marble and amphibolites, the Lesser Himalayan Zone is primarily composed of schist, phyllites, quartzite, and augen gneiss of granitic origin. Similar to the Lower Himalayan Zone, the Higher Himalayan Zone is primarily made up of kyanite, garnet, sillimanite bearing banded high-grade gneiss, interbedded with quartzite (Dhital, 2015).

Geologically, the study area is mostly composed of rocks from the Midland Group. The Lesser Himalayan Zone in the research area consists of the Lakharpata Sub-group and Dailekh Sub-group of the Mid-Land group (Dhital, 2015). The Dailekh Subgroup includes the Naudanada Formation, which is made up of fine-grained to medium-grained white quartzites, and the Ghanpokhara Formation, which is made up of black carbonaceous phyllites, slates, and shale with white limestones (Dhital, 2015). Similarly, the Lakharpata Subgroup consists of Sangram Formation, which is abundant in black laminated shales with interbeds of limestone and quartz, the Galyang Formation, which consists of black slates, and the Syangja Formation, which comprises calcareous quartzites and dolomitic limestones (Dhital, 2015).

3.2 Data types

The detail of the datasets and their sources used in this study is explained below.

3.2.1 Landslide Point and Polygon Data

In this study, Landslide inventory point datasets were collected by directly visiting the site of the study area by using GPS. Later landslide polygon layers were prepared by digitizing

area of landslides from Google Earth Pro. Landslides polygon were digitized from the image which were capture from the date of 2018-04-14 from to 2022-11-03.

3.2.2 Sentine-2 image

Part of the European Commission's Copernicus initiative, SENTINEL-2 was launched on June 23, 2015, with the aim of providing an abundance of data and imagery. The satellite features a opto-electronic multispectral sensor that can survey with a resolution ranging from 10 to 60 meters in the visible, near infrared (VNIR), and short-wave infrared (SWIR) spectral ranges, and includes 13 spectral channels. This capability allows for the detection of variations in vegetation, including changes over time, while also minimizing the effects of atmospheric conditions on image quality (Sentinel-2, 2021). The Level 2A product offers atmospherically adjusted Surface Reflectance (SR) images, obtained from the associated Level-1C products. Two scene of Level 2A captured on April 25, 2022 were downloaded from https://scihub.copernicus.eu/ website. From these products LULC map was prepared.

3.2.3 ALOS PALSAR Dem and its derivatives

In order to observe and explore the Earth, the Advanced Land Observation Satellite (ALOS), created by the Japanese Aerospace Exploration Agency (JAXA), was launched in 2006. To help with these activities, ALOS is equipped with three sensors: PRISM, AVNIR-2, and PALSAR. Shakya et al. (2018) claim that PALSAR (SAR) is an L-Band Synthetic Aperture Radar sensor with a 10-meter resolution that can operate in all weather conditions. In the present research ALOS PALSAR DEM data having 12.5m resolution was used, which was obtained from https://asf.alaska.edu/ website. Slope, Aspect, Curvature, Elevation, Topographic Wetness Index and Flow accumulation were derived from DEM.

3.2.4 Road networks

In this study, road networks datasets was downloaded from

https://data.amerigeoss.org/dataset/nepal-road-network-main-roads website. The dataset provided is a subset of OpenStreetMap data, containing only roads and adhering to the United Nations Spatial Data Infrastructure Transport (UNSDI-T) standards, prepared by the World Food Program (WFP). The dataset excludes streets and pathways and was last updated on August 8, 2019 (AmeriGEOSS, 2019).

3.2.5 Climatic Data

Comprising of gridded climate data in GeoTiff format, WorldClim is a global climate dataset used for spatial modeling and cartography. The second edition of WorldClim presents gridded climate data for each month's average from 1970 to 2000, with diverse geographic resolutions that range from 30 seconds (1 Km^2) to 10 minutes (340 Km^2) (WorldClim, 2021). There are 19 climatic variables which are in the form of GeoTiff raster format. However, only mean annual precipitation data download from WorldClim database (http://www.worldclim.org/bioclim) was used in this study. This data has 1Km of spatial resolution.

3.2.6 Geology

The geological map of Nepal was downloaded from **http://rds.icimod.org** website. Geological map of Nepal was prepared by ICIMOD by using geological Map of 100000 scale published by Department of Mines and Geology in 1994. It was last updated in 2020.

Table 1: Summary of datasets used in research

Data	Description	Source	Type
Landslide inventory (point and polygon)	Collected from directly site visit and Google Earth Images	Google Earth	Vector
Road network (OSM)	All the main road networks (Except streets and path ways)	**https://data.amerigeoss.org/dataset/nepal-road-network-main-**	Vector

		roads	
Land Use Land Cover	Obtained by Supervise Classification from Sentinel-2 Level-2A (10m*10m)	https://scihub.copernicus.eu/	Raster
ALOS PALSAR DEM (2007)	Downloaded (12.5m*12.5m)	https://asf.alaska.edu/	Raster
Slope, Aspect, Curvature, Drainage network	Derived from DEM (12.5m*12.5m)	https://asf.alaska.edu/	Raster
Topographic Wetness Index (TWI)	TWI=ln(CA/tan *slp)* *Where,* CA=Catchment Area and slp= slope gradient.	Raster calculator too	
Geology (lithology)	Geological map of Nepal prepared by ICIMOD by using geological Map of 100000 scale published by Department of Mines and Geology in 1994.	http://rds.icimod.org/	Vector
Distance from stream and road networks	Euclidean distance function was applied for calculating the distance from the stream and road networks.	Euclidean Tool	Raster
Precipitation	WorldClim (1km*1km) (Mean annual precipitation)	https://www.worldclim.org/data/worldclim21.html	Raster

3.3 Software used

ArcGIS Pro 2.4 and SNAP Desktop (Sentinel tool boxes) was used for Spatial data analysis and Landslide Mapping. SNAP tool was used to subset the area of interest and resampling the Level 2A product while mosaicking, compositing, rasterizing, clipping, etc. functions were performed by using ArcGIS Pro 2.4.

3.4 Methodological flow chart of study

This is the part of research work which clearly provides the sequence of steps for completion of the final output of the study/research. It also gives the clear ideas about the different types of factors and data used, data processing techniques and method applied for the research purposes in a single frame. Figure 1 is the methodological work flow of the study. It demonstrates various causative factors, such as slope, aspect, curvature,

TWI, distance to road, distance to drainage, precipitation, LULC, lithology, and elevation derived from various sources, have been taken into consideration when creating the landslide susceptibility maps using the FR and AHP methodologies.. Moreover, figure1

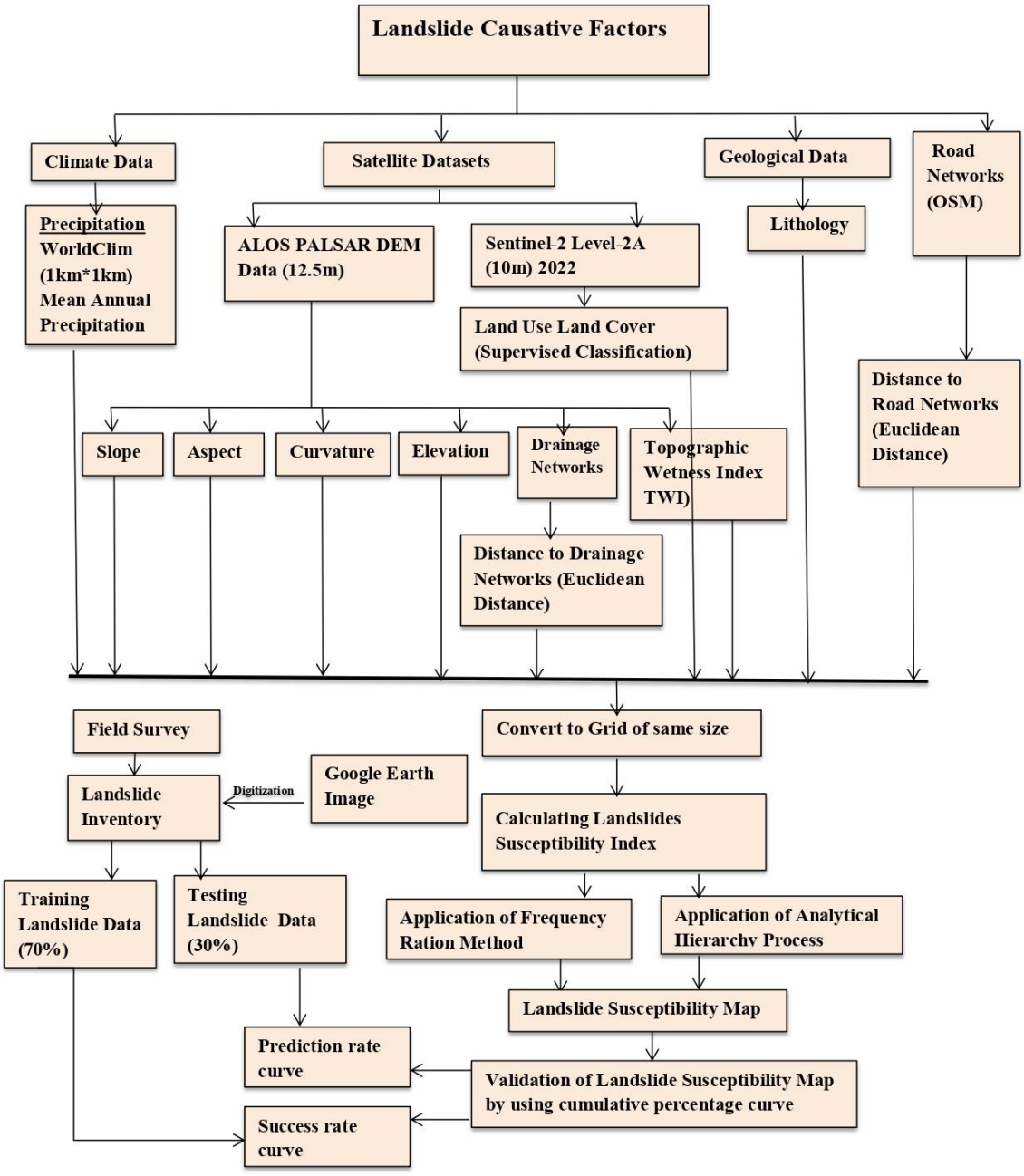

Figure 1: Methodological flow chart of the study

displays that the Landslide Susceptibility Maps have been validated by using cumulative percentage area curve method where training landslide data has been used for creating

success rate curve while testing landslide data has been used for creating prediction rate curve.

3.5 Selection of landslide causative factors and data preparation

A number of land-related factors are required for landslide susceptibility mapping and analysis. Studies from the several literatures revealed the use of a variety of landslides related parameters such as lithology, slope, aspect, curvature, elevation, land use/cover types, and drainage density for landslide risk mapping (Dai and Lee, 2002). Moreover, some additional parameters such as distance to road or settlements, normalized difference vegetation index, topographic wetness index (TWI), lineaments and soil types have been found to be used for susceptibility mapping (Pradhan and Lee, 2010). Pokharel and Thapa (2019) developed a model to determine the susceptibility of landslides in the Rasuwa District, which factored in slope, aspect, elevation, geology, peak ground acceleration (PGA), landuse, drainage proximity, and thrust proximity as contributing factors.

In this research ten landslide causative factors/elements were examined for Landslide Susceptibility Mapping (LSM) based on a review of the literature. They are Slope, Elevation, Aspect of Slope, Curvature, Distance from Stream, Distance from road, Topographic Wetness Index, Lithology, Rainfall and Land Use Land Cover (El Jazouli et al., 2019; Arsyad and hamid, 2020; Saha et al., 2020; Kumar & Anbalagan, 2016; Pokharel & Thapa, 2019; Panchal & Shrivastava, 2022; Demir et al., 2012; Reis et al., 2011; Park et al., 2012).

3.5.1 Slope

Due to the fact that shear pressures are directly impacted by the slope gradient, the slope angle is the main element used in slope stability calculations (Lee and Min 2001). The probability of sliding increases as the slope steepens (Lee and Min 2001). The slope's form is a key in triggering a landslide as it strongly influences on creating slope instability. The research study of Dai and Lee (2002) had shown that slope is a major landslides

causative factor. The soil becomes more susceptible to failure as the slope gradient increases due to increased soil stress (Saha et al., 2002). A steeper slope increases the likelihood of slope instability, which can lead to a landslide (Oh and Lee, 2010; Sharma et al., 2011).

In this research, slope map was derived from ALOS PALSAR DEM of 12.5 m resolution by using ArcGIS Pro software and was categorized into seven classes: <10, 10-20°, 20-30°, 30-40°, 40-50° and >50° which is shown in Map 4.

3.5.2 Aspect of slope

The angle of the steepest slope on the ground surface is referred to as the aspect. It refers to the slope direction, which is measured in degrees from 0° to 360° in a clockwise direction, with 0°, 90°, 180°, and 270° representing the slopes facing north, east, south, and west, respectively. Some of the parameters associated to aspect responsible for triggering of landslides are exposure to sunlight, rainfall, drying winds and discontinuities (Dai et al., 2001). The stability of terrain surfaces is significantly affected by aspect, which regulates soil moisture content and vegetation growth according to the amount of sunlight the terrain surface receives (Dahal, 2013).

In this study, aspect of slope was derived from ALOS PALSAR DEM by using ArcGIS Pro and was categorized into nine classes: Flat, North, East, South, West, Northeast, Southeast, Southwest and Northwest which is shown in Map 5.

3.5.3 Elevation

An elevation is another important factor which play significant role while conducting landslide susceptibility assessment. Dai and Lee (2002) has utilized elevation data as crucial data for effective landslide susceptibility mapping. It has inverse relationship with temperature and rainfall i.e. with the increase in elevation temperature and rainfall decreases and this relation is essential for plant growth and development in different elevated zone. The frequency of landslides on slopes in general increases with a rise in

rainfall, snowfall, and the strength of freeze-thaw cycles at higher altitudes (Lin and Tung, 2004).

In this study elevation map was derived from ALOS PALSAR DEM data ArcGIS Pro software and was classified into six classes: <1000m, 1000-1500m, 1500-2000m, 2000-2500m, 2500-3000m and >3000m which is shown in Map 7.

3.5.4 Curvature profile

The curved shape of the slope is known as the slope curvature. It significantly affects the direction and accumulation of water movement. When there is rainfall in the terrain surfaces, water flows from convex curvature and deposited to the concave curvature. This phenomenon is known as flow accumulation and accumulated area are highly prone to landslide incident (Dahal, 2017). Concave slope has positive value whereas convex slope gives negative curvature value.

ArcGIS Pro software was used to derive the curvature profile of the research area from the ALOS PALSAR DEM, which was divided into five classes.: -23.20 to -2.00, -2.00 to -0.50, -0.50 to 0.35, 0.35 to 1.64 and 1.64 to 31.41 which is shown in Map 6.

3.5.5 Geology (Lithology)

Lithology, a key factor, has a direct impact on the incidence of landslides. The impact of geology on landslides is widely acknowledged, as differences in the durability and permeability of rocks and soils caused by lithological and structural variations can lead to such occurrences (Ayalew & Yamagishi, 2005). As the composition and structure of different rocks are different that contributes to the slope materials strength in a positive and negative ways. Greater resistance is offered by stronger rock formations against driving forces as compared to weaker ones. Therefore, Dai and Lee (2002) and Ayalew et al. (2005) have considered lithology as a crucial input factor for landslides susceptibility mapping. The research sites contain a variety of rocks, including slate, phyllite, schist, quartzite, limestone, marble, and dolomites.

Geological map of Nepal prepared by ICIMOD by using geological Map of 100000 scale published by Department of Mines and Geology in 1994 was used in the current study. Sixteen geological classes were identified. They are Himal group, Ghanpokhara formation, Ranimatta formation, Ulleri formation, Sangram formation, Gn, Naudanda formation, Galyang formation, Sh, Udayapur formation, Rb, Chandragiri formation, Recent, Tistung formation, Sopyang formation and Upper siwalik which is shown in Map 11.

3.5.6 Land use land cover

Land cover is most sensitive factors which can be easily affected by the human activities and change in environment condition. The implementation of effective land use practices promotes the stability of hilly slopes by regulating the pace of weathering and erosion of the underlying rock formation. Land cover always controls landslide process. Slope covered with forest and best land use practiced are less prone to landslides occurrence but slope with no any vegetation or barren land have high risk of slope failures.

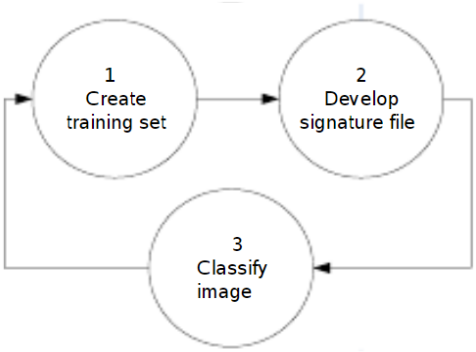

Figure 2: Supervised Classification steps

In the present study, Sentinel 2-Level-2A imagery was used for Land Use Land Cover Mapping. Supervised classification method was used where Maximum likelihood was used as classifier algorithm for Classification of Image (Esaid et al., 2018). Prior knowledge of the research area is used in supervised classification approaches, which is highly beneficial in obtaining better classification (Esaid et al., 2018). The research area was classified into seven classes: Forest, Grassland, Cropland, Water bodies, Barren Land, River bed and Built-up areas which is shown in Map 10.

Accuracy Assessment of classified image

In this step, I have used 500 randomly selected points and implemented a stratified random sampling method to measure the accuracy of the products. The accuracy assessment of the classified image obtained from supervised classification was carried out in ArcGIS pro software where the confusion matrix was derived. The ground truth information was obtained using visual interpretation high quality satellite images. Later, these assessment tools generated the error matrix which determines the users, producers, overall accuracy, and the Kappa accuracy level.

Additionally, the results of the producer's accuracy, which displays how well the training set pixels are classified for specific LULC types, and the user's accuracy, which displays the probability of the classified pixels that represent the ground data, were derived. Similarly, Kappa statistics which shows how well the classification is compared with randomly assigned class value to each pixel was also attained. The overall class accuracy was evaluated using the Kappa statistics, which provides a statistically accurate assessment of the quality of classification (Esaid et al., 2018).

3.5.7 Distance to road networks

Distance to road is another controlling factor for landslides incident. The occurrence of landslides is strongly correlated with it. Opening new routes and expansion of existing roads both disturb the natural topology and affect the slope stability. Continuous vehicle movement and slope stability changes during road construction may cause the slope to become unstable (Yalcin et al., 2011). The crack in the slope cutting absorb large volume of water which induces oversaturation of water content in the soil and lead to sliding of sloppy land.

In the present study, distance raster map was prepared by using Euclidean distance analysis tool available in ArcGIS Pro. Road distance raster was classified into six classes based on the assumption that distance closer to road networks are more prone to landslides: <100m, 100-200m, 200-300m, 300-400m, 400-500m and >500m which is

shown in Map 13.

3.5.8 Distance to drainage networks

Distance to drainage is another geomorphology related landslides causative factor. The level of saturation of the slope's material governs a slope's stability. The stability of the slope may suffer if the slopes erode continuously or if the lower part of the materials becomes saturated until the water level rises. (Dai et al., 2002; Saha et al., 2002).

Distance to drainage map was created by using Euclidean distance method (El Jazouli et al., 2019). Natural drainage of the research area was generated by hydrological analysis. Starting with hydrological fill modeling using a DEM, the process progressed to the calculation of flow direction and concluded with flow accumulation (Arsyad & Hamid, 2020). Flow accumulation was converted to stream features and Euclidean distance analysis was performed for creating distance to drainage.

Drainage distance raster was classified into eight classes based on the assumption that distant closer to stream networks are more prone to landslides:<50m, 50-100m, 100-150m, 150-200m, 200-250m, 250-300m, 300-350m and >300m which is shown in Map 12.

3.5.9 Precipitation

Rainfall is an essential extrinsic variable used in susceptibility analysis. In statistical landslide susceptibility analysis the spatially distributed average annual rainfall is commonly used (Dahal, 2008). Bioclimatic variables from the present (1970–2000) were downloaded for the study from WorldClim-Global Climate Data (www.worldclim.org/bioclim). There were 19 bioclimatic variables of the entire world which were received in a grid format with spatial resolution of around 1km. Among those variables only Mean annual Precipitation layers were applied. Precipitation map of the study area was classified into seven classes: 845-1000mm, 1000-1200mm, 1200-1400mm, 1400-1600mm, 1600-1800mm, 1800-2000mm and 2000-2214mm which is

shown in map 9.

3.5.10 Topographic Wetness Index (TWI)

Different values of TWI affect the soil moisture and species, thus TWI calculated from DEM is widely used as a proxy for soil moisture (Kopecký et al., 2021). TWI takes into account the catchment area as well as the slope gradient. It is related to the accumulation of flow in the particular terrain (Kumar & Anbalagan, 2016). The biological processes including vegetation patterns, forest site quality and annual net primary production can be categorized based by using TWI (Beven & Kirkby, 1979; Sorenson, et al., 2006). In flat, convergent terrains, the wetness index is higher, while steep, divergent terrains have a lower wetness index. The level of moisture in soil can directly impact the stability of slopes, especially in regards to landslides. This is due to the effect of soil moisture on the slope material, which can cause an increase in pore water pressures and a decrease in soil strength (Kavzoglu et al., 2013). According to Kopeck et al. (2021), soil moisture regulates both environmental processes and species distributions. The wetness index is a widely used tool for assessing the role of topography in hydrological processes and provides insights into the links between topography and variations in rainfall (Beven and Kirkby, 1979).

It can be obtained using formula:

TWI=ln(CA/tan *slp)*

Where,

CA= Catchment Area and

slp= slope gradient.

Using the raster calculator function in ArcGIS Pro, the TWI map for this study was created by starting with a DEM and applying the above relationship. TWI of the study area was classified into five classes as per natural break (jenks) classification method: 1.01 - 4.69, 4.69 - 6.57, 6.57 - 9.40, 9.40 - 14.40 and 14.40 - 25.05 which is shown in Map 8.

3.6 Image Pre-processing

3.6.1 Compositing and Mosaicking Bands

Before performing Compositing and Mosaicking, each band of Sentinel-2 Level-2A was subset to the area of interest and resampled to the pixel of 10m by using SNAP software and was saved in ENVI file format. After that, resampled imageries were used for compositing band to create single image by using ArcGIS pro software. After that, composited band image from the previous method was used for mosaicking two image layers to create single continuous image. Similarly, two DEM Image layers were also stacked to perform continuous DEM image for the study area.

3.7 Data Processing

3.7.1 Clipping

Clipping is the process of extracting data of the required area of interest. Clip function helps in clipping the extent of one geographical layer with the extent of another geographical layer. In this study, all the datasets were clipped with an extension of study area.

3.7.2 Rasterization

Rasterization is the process of converting vector form data (point, line and polygon) into raster form (composed of pixels). The crucial tool that aids in converting polyline and polygon data to raster is the conversion tool for polylines and polygons. In the present study, Geology and Landslides polygons datasets were rasterized by using polygon to raster function by defining the cell size of 10m.

3.7.3 Resampling

The raster object is produced using the resampling method, which modifies the input raster's spatial resolution by creating rules for aggregating or interpolating data over the new pixel sizes. This method is known as resampling. Four different types of resample

function are available in ArcGIS pro: Nearest Neighbor, Majority Algorithm, Bilinear Interpolation/Bilinear Interpolation Plus and Cubic Convolution.

In this study, DEM and precipitation datasets were resampled by using nearest neighbor resampling technique with the output cell size defined as Sentinel 2 Level 2A (10m). The fastest interpolation technique is nearest neighbor, which preserves the cells' initial values and is appropriate for discrete data like land use classification (ESRI, 2021).

3.7.4 Size of grid

In this study all the datasets required for the study area were maintained to 10m of resolution. DEM and its derivatives, distance raster datasets, geology, precipitation and landslides inventory polygon datasets were maintained to 10m resolution by applying resampling tool available in ArcGIS Pro.

3.7.5 Coordinate System Projection

All the datasets were in WGS 1984 coordinate system, so all those datasets were projected from WGS 1984 to WGS 1984 UTM Zone 45N Projected Coordinate System for further statistical calculation and analysis.

3.8 Landslides Inventories and Mapping

For a detailed study of landslide susceptibility assessment, information related to landslides events needs to be collected, which can be done by creating a landslide map (Nayak, 2010). The fundamental type of landslide mapping is known as a landslide inventory, which involves documenting the location, date, and visible evidence of landslides within a particular area (Wieczorek, 1984). Depending on the scope of the study area, intended use, resources available, and scale of base maps and aerial photographs, various methods and approaches can be used to create inventory maps for landslides, according to Guzzetti et al. (2000). In the present study, landslide point datasets were collected by directly visiting the sites, and polygons were later mapped by digitizing high-quality satellite images from Google Earth Pro. The number of landslides

that occurred and the number of landslide pixels in different classes of factors were calculated using the zonal statistic as table tool available in ArcGIS Pro. Firstly, both the landslide point and polygon datasets were converted to raster format using the conversion tool, and then the zonal statistic as table tool was used to calculate the landslides events and the area of landslide in each factor's class.

3.9 Landslide Susceptibility Mapping

In the present study, Landslide Susceptibility Index map of the research area was prepared by using AHP and FR Methods for the comparative assessment.

3.9.1 Analytical Hierarchy Process

Saaty introduced the Analytical Hierarchy Process in 1980, a method of multi-criteria decision-making approach that employs pair-wise comparisons and expert opinions to establish priority scales (Saaty, 2008). AHP operates on four stages, namely defining the problem, selecting goals and options, creating pair-wise comparison matrices, determining weights, and establishing the overall priority (Pardeshi et al., 2013. The weighting/rating of factors and their classes by using the AHP technique offers several benefits but also some drawbacks. It offers a structural foundation for measuring pair-wise comparisons of choice factors and criteria. This type of comparison considerably minimizes complexity and improves decision-making simplicity (Sadasivuni et al., 2009). The relative weighting of the criteria heavily relies on an individual's or professional's understandings. Overlooking the importance that an individual or professional assigns to a factor is a significant flaw of subjective decision-making systems (Kumar and Anbalagan, 2016). Pairwise comparison, however, provides a simple and acceptable decision-making rule, according to Kumar and Anbalagan (2016). According to Yalcin (2008), the AHP method enables obtaining a score judgment by drawing upon professional knowledge/experience, which may be either subjective, objective, or a blend of the two.

3.9.1.1 Weighting value for factor/factor's classes

In the present study, relative preference value for all the factors were calculated mainly based on landslide inventory and field observation, review from literatures (Veerappan et al., 2017; Agrawal & Dixit, 2022; Quan & Lee, 2012; Kayastha et al., 2013; Kavzoglu et al., 2013; Achour et al., 2017; Yalcin et al., 2011) and expert opinion. Similar to this, percentages of the landslide area within each class of factors were used to determine the relative value for each class of factors (Agrawal & Dixit, 2022; Quan & Lee, 2012). Saaty's preference and judgement scale was used for assigning the relative preference value to factors/factors' class (Agrawal & Dixit, 2022; Quan & Lee, 2012). Table 3 shows the preference value ranges from 1 to 9. Finally, weighted values for factors/factor's classes were calculated by forming pairwise comparison matrix table based on Saaty's rating scale by using AHP methods. All the essential steps from formation of pairwise comparison matrix to calculation of weight and CR is explained below as an equation: (Sadasivuni et al., 2009).

For a pairwise element matrix;

$$\begin{bmatrix} C_{11} & C_{12} & C_{13} \\ C_{21} & C_{22} & C_{23} \\ C_{31} & C_{32} & C_{33} \end{bmatrix} \qquad \text{……Equation 1.}$$

To produce the normalized pairwise matrix, first add values to the pairwise matrix and divide each element by the sum of the columns

$$\begin{bmatrix} X_{11} & X_{12} & X_{13} \\ X_{21} & X_{22} & X_{23} \\ X_{31} & X_{32} & X_{33} \end{bmatrix} \quad X_{ij} = \frac{C_{ij}}{\sum_{i=1}^{n} C_{ij}} \qquad \text{……Equation 2.}$$

After that, the weighted matrix was created by dividing the total of the normalized rows by the number of criteria/factors.

$$\begin{bmatrix} W_{11} \\ W_{21} \\ W_{31} \end{bmatrix} \quad W_{ij} = \frac{\sum_{j=1}^{n} X_{ij}}{n}$$ ……Equation 3.

Steps to calculate the Consistency Ratio (must be made less than 10%) is as follows:

$$\begin{bmatrix} C_{11} & C_{12} & C_{13} \\ C_{21} & C_{22} & C_{23} \\ C_{31} & C_{32} & C_{33} \end{bmatrix} * \begin{bmatrix} W_{11} \\ W_{21} \\ W_{31} \end{bmatrix} = \begin{bmatrix} C_{v_{11}} \\ C_{v_{21}} \\ C_{v_{31}} \end{bmatrix}$$ ……Equation 4.

The calculation for the consistency vector involved dividing the weighted sum vector by the criterion weight, which yielded the following result:

$$C_{v_{11}} = \frac{1}{W_{11}}[C_{11}W_{11} + C_{12}W_{21} + C_{13}W_{31}]$$
$$C_{v_{21}} = \frac{1}{W_{21}}[C_{21}W_{11} + C_{22}W_{21} + C_{23}W_{31}]$$
$$C_{v_{31}} = \frac{1}{W_{31}}[C_{31}W_{11} + C_{32}W_{21} + C_{33}W_{31}]$$ ……Equation 5.

Following the calculation of the Consistency Vector, Lambda (λ) was determined by averaging the Consistency Vector's value. The Consistency Index (CI) gives a measurement of divergence from consistency.

Consistency Ration:

CR= (CI/RI)

CI= (λ_{max}-m/m-1)

Where λ_{max} = maximum eigenvalue; m= total number of causative factors, and RI= random index.

A random index (table 2) was created using a number of random samples (Saaty, 1980). The weighting/rating values for all contributing factors and factors' classes were calculated by using AHP- Online System (AHP-OS). The pairwise comparison is regarded as consistent if the CR values are lower than 10% (Panchal & Shrivastava, 2021). So, the evaluation process was repeated until the consistency ratio was maintained below 10%.

Table 2: Random consistency Index (Saaty, 1980)

N	1	2	3	4	5	6	7	8	9	10	11	12	13	14	15
RI	0	0	0.58	0.9	1.12	1.24	1.32	1.41	1.45	1.49	1.51	1.53	1.56	1.57	1.59

Table 3: Preference and Judgement Scale (Saaty, 1980)

Preference/ ordinal scale	Degree of preference	Remarks
1	Equally	Factors inherit equal contribution
3	Moderately	One factor moderately favoured over other
5	Strongly	Judgement strongly favour one over other
7	Very strongly	One factor very strongly favoured over other
9	Extremely	One factor favoured over other in highest degree
2,4,6,8	Intermediate	Compensation between weights 1,3,5,7 and 9
Reciprocals	Opposite	Refers inverse comparison

3.9.1.2 Landslide Susceptibility Index from AHP method

From the literature review, the general equation for creating LSI map is shown below (Saha et al., 2002; El Jazouli et al., 2019; Pokharel & Thapa, 2019; Kumar & Anbalagan, 2016; Yalcin & Bulut, 2006; Arsyad & Hamid, 2020);

$$LSI = \sum_{i=1}^{n} (R_i * W_i) \quad \text{.....Equation (6).}$$

Where,

LSI= Landslide Susceptibility Index

$\mathbf{R_i}$**=** Rating class of each layer,

$\boldsymbol{W_i}$ **=** Weights of each landslide causative factors.

In this research, equation 6 was applied in for generating LSI map by using raster

calculator function available in ArcGIS Pro 2.4.

3.10 Frequency Ratio method

The Frequency Ratio is a statistical tool that examines the links between the distribution of landslides and their causal elements in a bi-variate manner to assess landslide susceptibility (Yalcin et al., 2011). By utilizing this technique, it is possible to ascertain the spatial relationship between the occurrence of landslides and the factors that contribute to them. This methodology involves determining the frequency ratio of a subclass of each causative factor, based on its association with landslides. The FR of a subclass of each causative factor was calculated by using following equation (Saha et al., 2020);

Equation,

$FR=(f/tf)/(x/tx)$ …….....Equation (7)

Where,

f = number of landslide pixels in subclass of landslide conditioning;

tf = total number of landslide pixels;

x = total number of pixels in the subclass of landslide-conditioning factor; and

tx = total number of pixels

When the FR value exceeds 1, it implies a strong correlation between landslides and factors, but a value less than 1 indicates a weaker correlation (Regmi et al., 2014).

3.10.1 Landslide Susceptibility Index from Frequency Ratio method

The Landslide Susceptibility Index was computed by adding up the raster datasets generated from the application of frequency ratio based on equation (7) (Rasyid et al., 2016).

$LSI= Fr_1+Fr_2+Fr_3+….+Fr_n$ .....Equation (8).

Where, LSI= Landslide Susceptibility Index,

Fr= Rating of each factor's class

Both techniques employed Jenk's natural break classifier to divide the LSI map into

various landslide susceptibility categories, including very low, low, moderate, high, and very high (El Jazouli et al., 2019). Jenk's natural break classifier aims to increase the variance across classes while decreasing the variance within classes (McMaster, 1997).

3.11 Assessment of LULC in different Susceptibility Classes

For assessing the important land cover of the study area like forest, built-up areas and cropland, LULC areas located in the different level of Susceptibility were calculate. Tabulate area function tool available in ArcGIS Pro 2.8 was used for calculating the area of LULC located in different classes of LSI map prepared from FR and AHP methods.

3.12 Validation of Landslide susceptibility Map

A range of statistical techniques can be used to evaluate model accuracy, such as ROC plot, error rate, success rate, and prediction rate curve (Kumar and Anbalagan, 2016). In this study, the accuracy of the landslide susceptibility map was confirmed by utilizing the success rate curve and prediction rate curve (Kumar and Anbalagan, 2016; Thapa & Bhandari, 2019). The success rate curve and prediction rate curve were created using 70% (153) and 30% (65) training and testing landslides, respectively (Thapa & Bhandari, 2019). For creating success rate curve and prediction rate curve, at first, LSI Maps were reclassified into 100 equal classes. The LSI maps that had been classified were organized in a descending sequence, and for each susceptibility class, the training pixels and testing landslide pixels were determined by applying the zonal statistics as a table tool (Sonker et al., 2022). The success rate curve was then created by graphing the cumulative percentage area of the training landslide on the Y-axis against the cumulative percentage area of the susceptibility map on the X-axis (Sonker et al., 2022). Similarly, a prediction rate curve was created by graphing the cumulative percentage area of the testing landslide on the Y-axis against the cumulative percentage area of the susceptibility map on the X-axis (Sonker et al., 2022). AUC was then calculated by using trapezoidal method for testing the accuracy assessment of LSI map (Thapa & Bhandari, 2019).

The formula for calculating AUC is shown below (Silalahi et al., 2019);

AUC = $\sum_0^n (X_i - X_{i-1})Y_1 - [(X_i - X_{i-1})((Y_i - Y_{i-1}))/2]$ ……..Equation (9)

Where,

AUC= Area Under a Curve

X_i= Percentage of the susceptibility area

Y_1= Percentage of Landslide area

Chapter-4: Results

4.1 Landslide Inventory

In the present study, 218 landslides events were recorded from field survey. 56 landslides were recorded as active landslide while 162 landslides were old landslide. The total landslide pixel from 218 landslide events was found to be 9936.

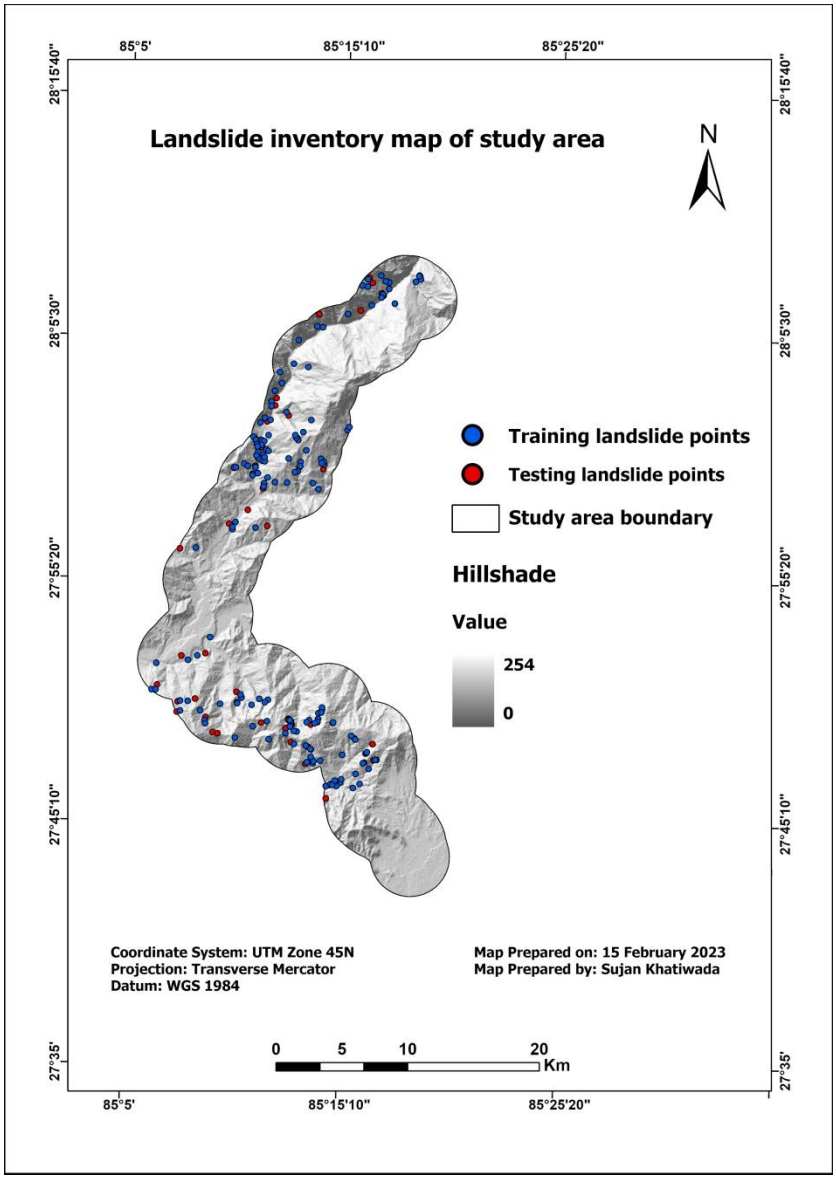

Map 2: Landslide point datasets of study area

From the inventory, the area of the landslide was found to be ranged from 36 to 74700 square meters. Smaller but frequent landslides were found to occur closer to road

networks but bigger landslides were found to occur above 500m distance from the road networks. Bigger landslides were mostly observed in Hakubesi village of Rasuwa district.

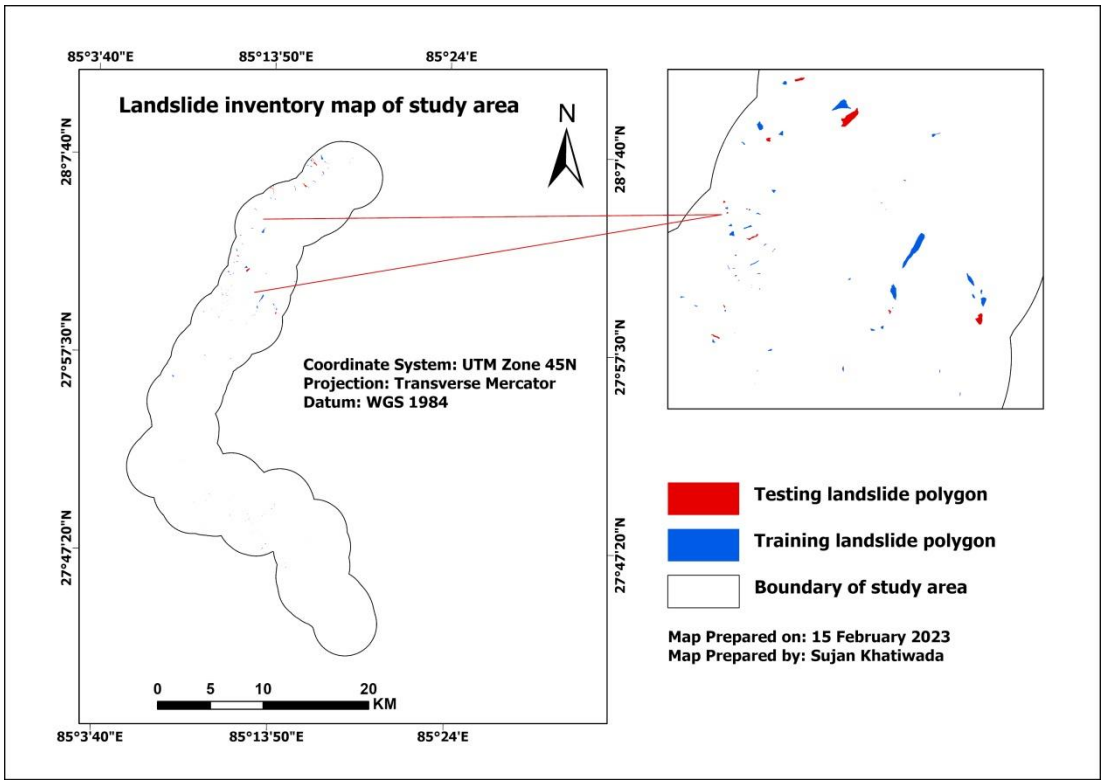

Map 3: Landslide polygon datasets of study area

4.2 Landslide causative factors

The current research examined a total of ten factors that contribute to landslides for the purpose of creating a Landslide Susceptibility Map. The distribution of landslides in each of the causative factor is presented below.

4.2.1 Slope

The presence of slope as a topographical feature is critical, as it impacts both the surface and subsurface hydrology and the stability of the land. Map 4 displays the distribution of landslide events in different slope classes. Table 4 reveals that the highest number of landslide events (85) occurred in the slope class of 30 to 40 degrees, which covered 42.95% of the total landslides, while the lowest percentage (0.20%) of landslides occurred

in slopes less than 10 degrees.

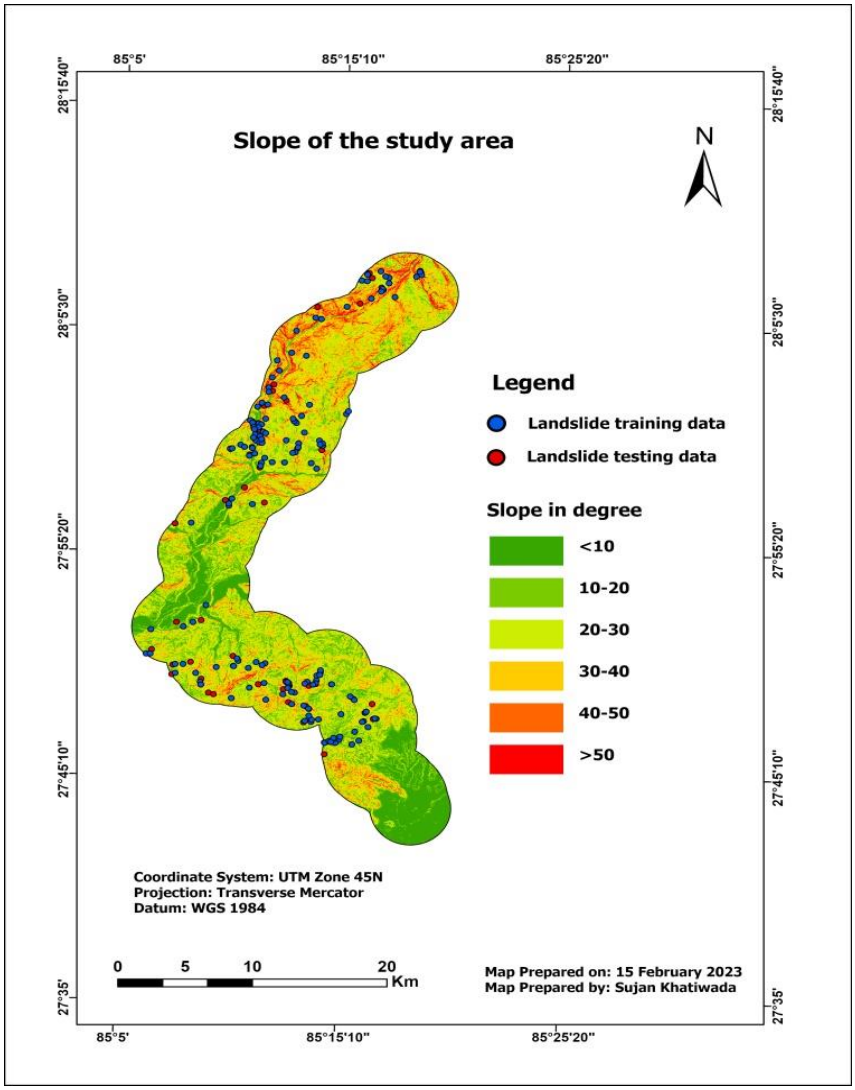

Map 4: Slope of the study area

Table 4: Landslides in different slope classes

Slope classes	No. of landslide	Landslide Pixels	Landslide area (%)
<10°	1	20	0.20
10°-20°	20	469	4.72
20°-30°	83	3213	32.34
30°-40°	85	4268	42.95
40°-50°	24	1659	16.70
>50°	5	307	3.09
Total	218	9936	100

4.2.2 Aspect

It is also a crucial factor that influences the solidity of terrain surfaces because It controls soil moisture and vegetation growth according to the surface of the ground exposed to the sun. The landslide distribution in different aspect classes is shown on Map 5.Table 5 shows that 41 landslide events were found on south-facing slopes, which covered a maximum landslide area of 34%. Additionally, Table 5 demonstrates that slopes facing southeast, south, and southwest were responsible for about 73% of the total landslide area.

Table 5: Landslides in different classes of aspect

Aspect classes	No. of landslide	No of landslide pixel	Landslide area (%)
Flat	1	3	0.03
North	16	118	1.19
Northeast	12	198	1.99
East	37	949	9.55
Southeast	41	3408	34.30
South	32	1773	17.84
Southwest	28	2274	22.89
West	34	851	8.56
Northwest	17	362	3.64
Total	218	9936	100

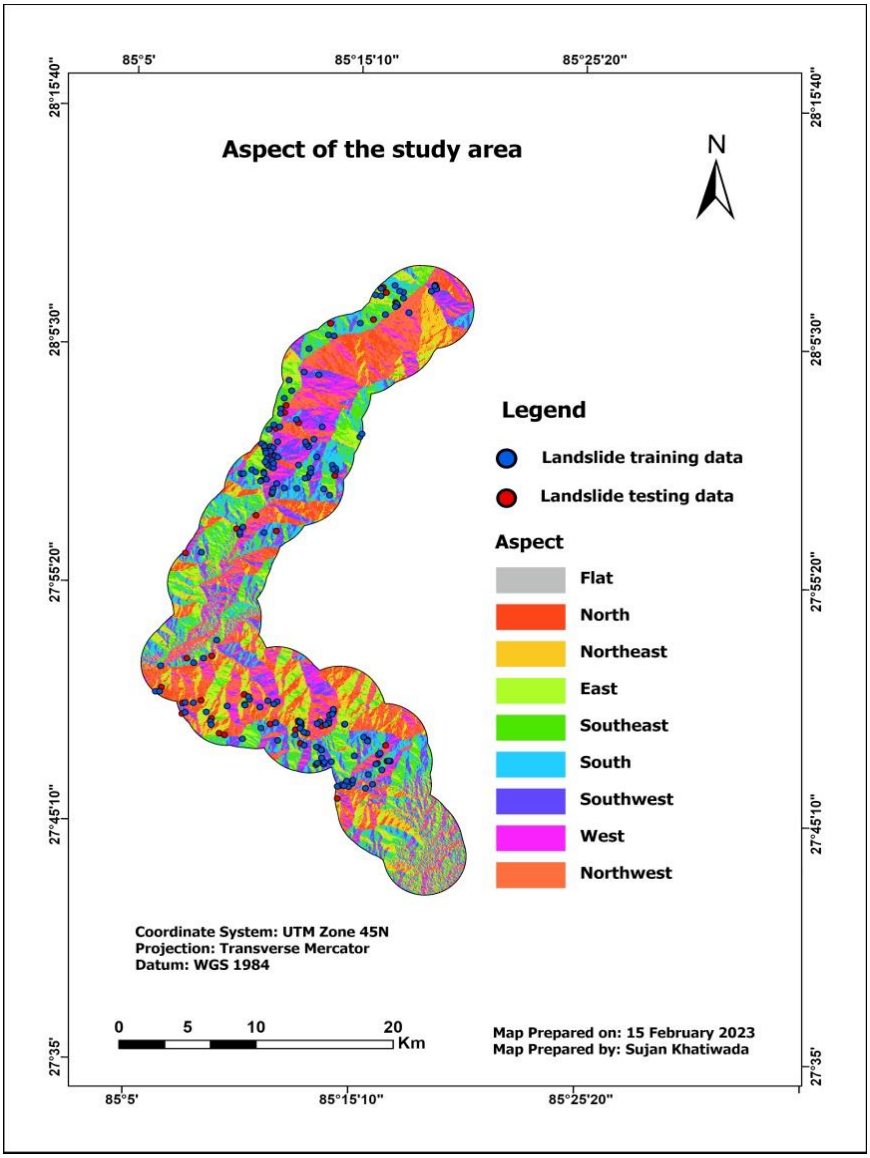

Map 5: Aspect map of the study area

4.2.3 Curvature profile

A slope's curved shape is referred to as its curvature. and it has a significant impact on water accumulation and movement. The distribution of landslide events across different curvature profile classes can be seen on Map 6. Table 6 shows that most landslide events (88) and the largest landslide-affected areas were observed in curvature classes from -0.50 to 0.35. The study also found that the maximum landslide area (38.18%) occurred in the curvature profile between -0.50 to 0.35, while the minimum numbers of landslides were recorded in the -23.20 to -2.00 curvature class.

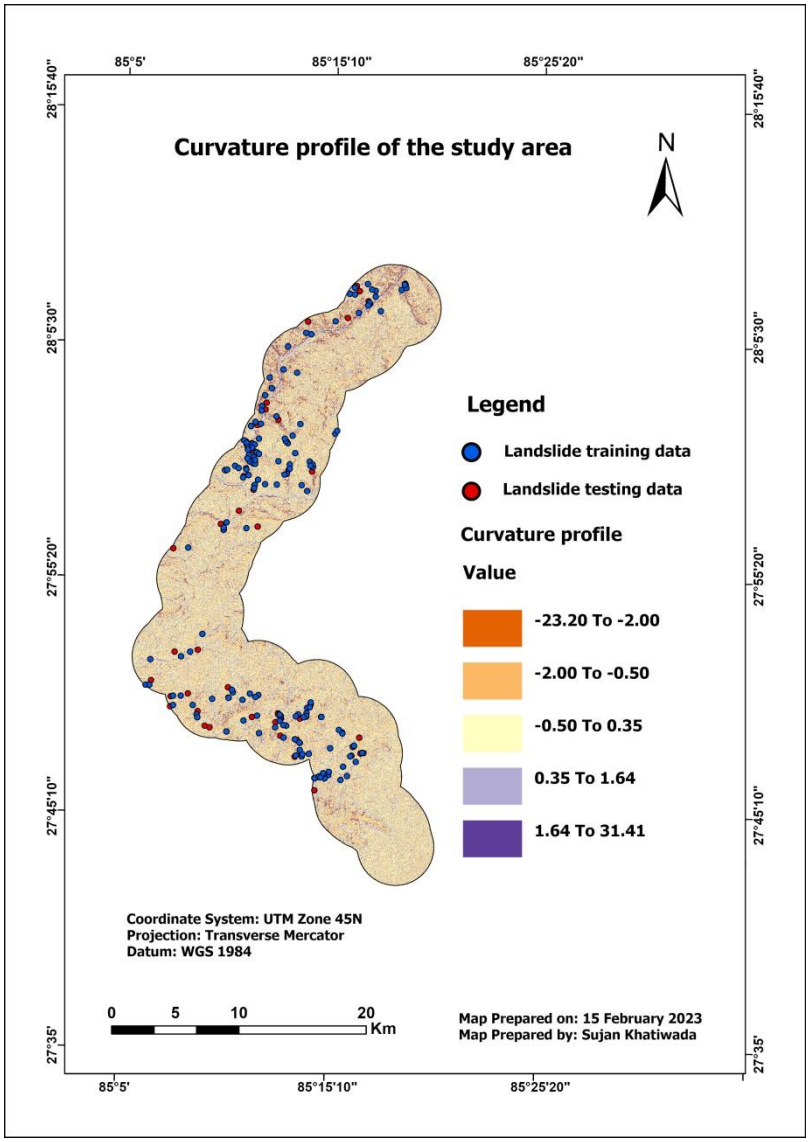

Map 6: Curvature profile of study area

Table 6: Landslides in different classes of curvature classes

Curvature profile classes	No. of landslide	No of landslide pixel	Landslide area (%)
-23.20 To -2.00	4	195	1.96
-2.00 To -0.50	38	2370	23.85
-0.50 To 0.35	88	3729	37.53
0.35 To 1.64	75	3067	30.87
1.64 To 31.41	13	575	5.79
Total	218	9936	100

4.2.4 Elevation

An elevation is another crucial factor that plays a significant role in conducting landslide susceptibility assessment. Map 7 shows the allocation of landslides across varying elevation categories within the studied location. The maximum numbers of landslides were found to occur at an elevation ranging from 1500 to 2000 meters, while no landslides were found at elevations above 2500 meters (Table 7). Furthermore, Table 7 also displays the maximum number of landslide pixels occur at elevations between 1500 to 2000 meters.

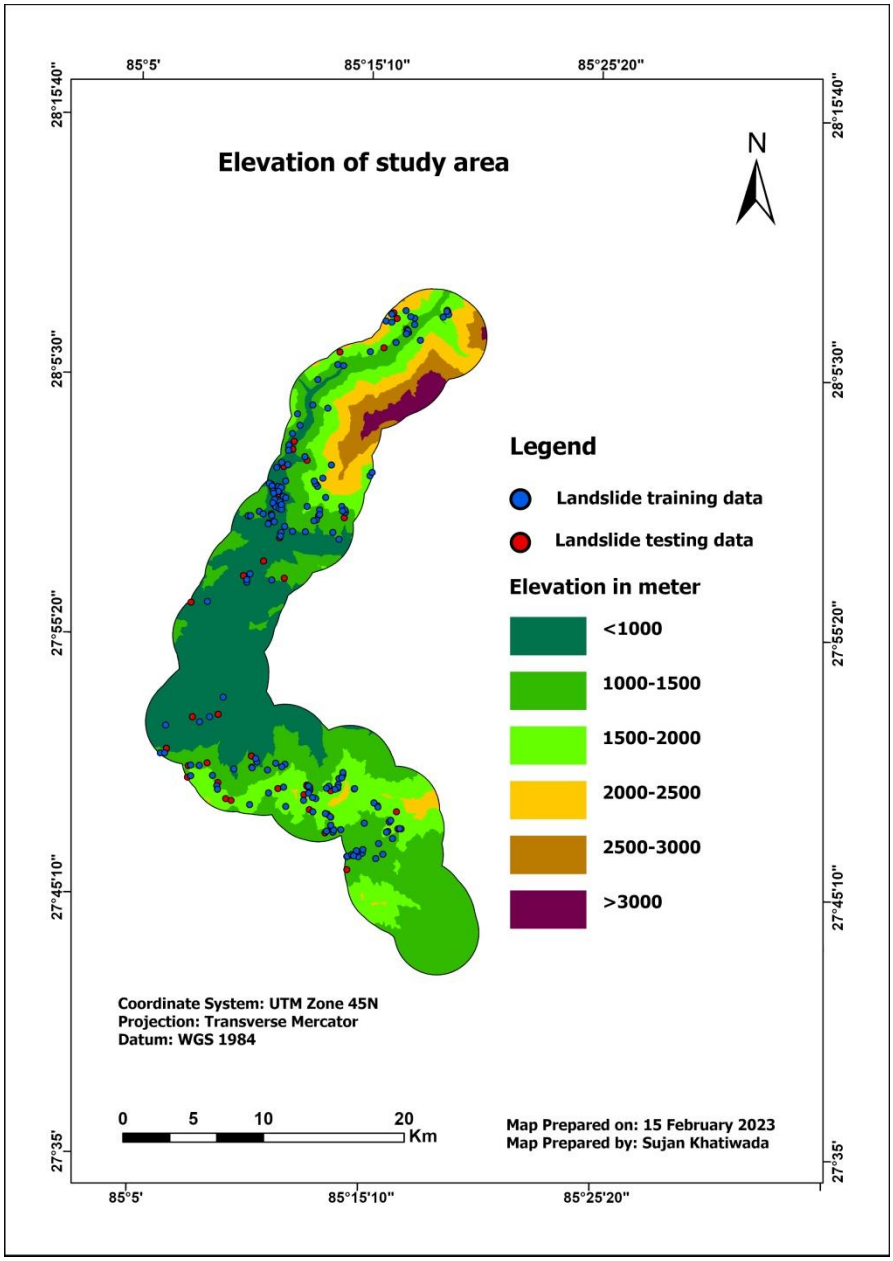

Map 7: Elevation Map of area

Table 7: Landslides in different elevation class

Elevation classes (meter)	No. of landslide	No of landslide pixel	Landslide area (%)
408-1000m	64	1689	17.00
1000-1500m	68	3644	36.67
1500-2000	82	3982	40.08
2000-2500	4	621	6.25
2500-3000	0	0	0.00
3000-3611	0	0	0.00
Total	218	9936	100

4.2.5 Topographic Wetness Index

TWI generated from DEM is a commonly used approach for estimating soil moisture, where varying TWI values exert control over soil moisture and species (Kopecký et al., 2021). Landslides distributions in different classes of TWI are clearly shown in the Map 8. Table 8 shows that maxim landslides (114) and maximum landslides pixels (4361) were found to occur in an area having TWI ranged from 4.69 to 6.57. Further table 8 shows that both the frequency of landslide and number of landslide pixels were found to be gradually decreasing from TWI 4.69 onward.

Table 8: Landslides in different TWI classes

TWI classes	No. of landslide	No of landslide pixel	Landslide area (%)
1.01 - 4.69	64	3254	32.75
4.69 - 6.57	114	4361	43.89
6.57 - 9.40	29	1880	18.92
9.40 - 14.40	10	438	4.41
14.40 - 25.05	1	3	0.03
Total	218	9936	100

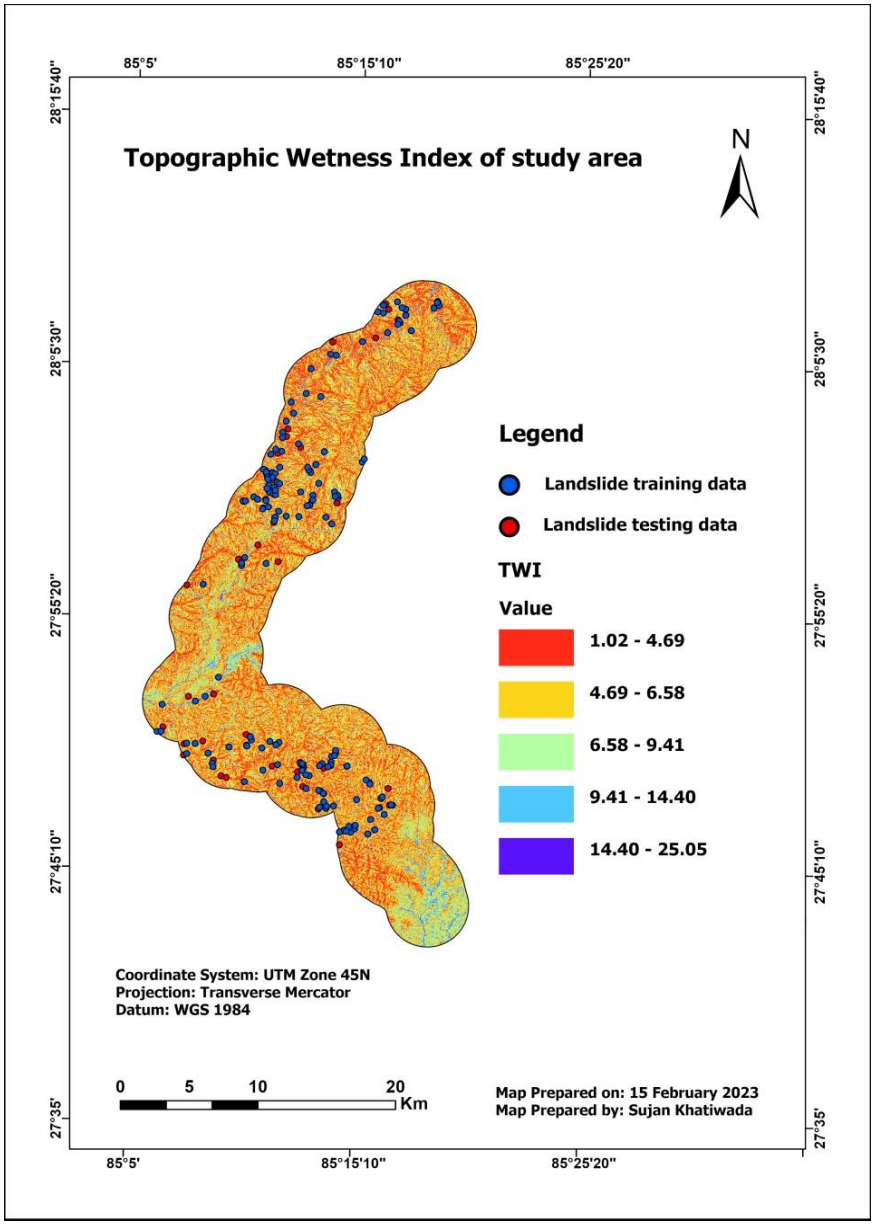

Map 8: TWI map of the study area

4.2.6 Precipitation

Precipitation serves as a vital extrinsic variable in landslide susceptibility analysis, where the average annual rainfall across a region is frequently employed in statistical models to assess susceptibility (Dahal, 2008). The presence of landslide in different precipitation range classes are shown in map 9. Table 9 shows that maximum landslides (95) were occurred in precipitation between 1800 to 2000 millimeters but 12.48% of landslide areas

were covered by 95 landslides. Moreover, Table 9 shows that bigger landslides were found to occur in an area receiving an annual precipitation of 1400 to 1600 millimeters. 5153 landslide pixels were found to occur in 1400-1600 millimeters of precipitation class from only 35 landslides events. Furthermore, table 9 also shows that no any landslide was observed in precipitation below 1200 millimeters.

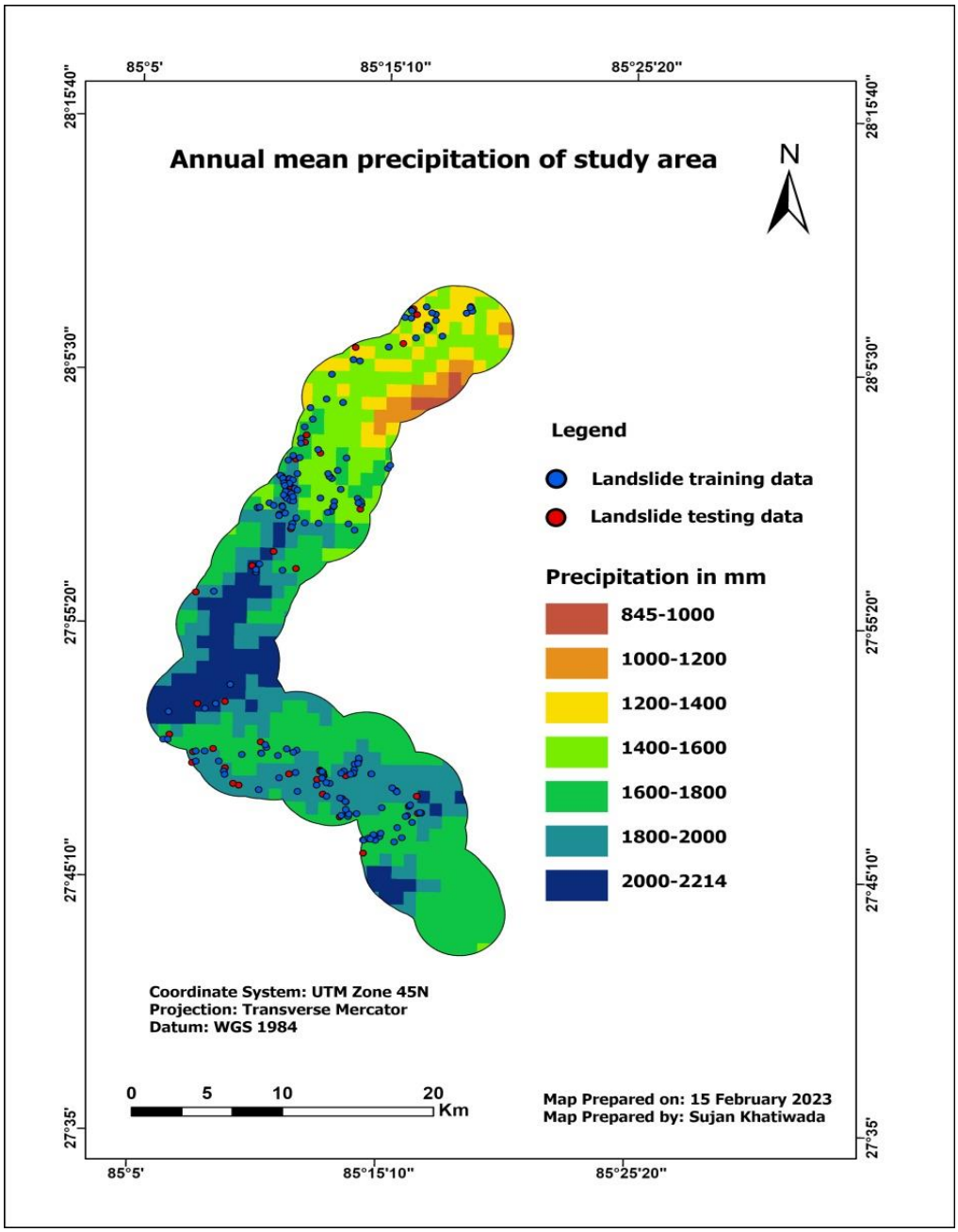

Map 9: Precipitation map of study area

Table 9: Landslide in different precipitation classes

Precipitation classes(millimeter)	No. of landslide	No of landslide pixel	Landslide area (%)
845-1000	0	0	0
1000-1200	0	0	0
1200-1400	13	1867	18.79
1400-1600	35	5153	51.86
1600-1800	66	1584	15.94
1800-2000	95	1240	12.48
2000-2214	9	92	0.93
Total	218	9936	100

4.2.7 Land Use Land Cover

Changes in environmental conditions and human activities can readily impact land use and land cover, rendering them critical determinants of landslide occurrence. It is also one of the crucial factors controlling the occurrence of landslides.

A supervised classification was carried out by using using Sentinel-2 Level-2A image to produce a LULC layer of the research area. The final reclassified LULC map is displayed in Map 10. It was found that the highest area was covered by forest (51.28%), followed by cropland (37.62%) and built-up areas (7.94%) (Table 10). Less than 1% of the area was made up of grassland, water, and riverbed, as shown in Table 10. The distribution of landslides in different classes of LULC is clearly presented in Map 10. It was found that the maximum landslide events (140) and landslide pixels (5466) occurred in cropland (Table 10). In a similar vein, Table 10 reveals that 65 landslide events—the second-highest number—were noted in forests.

Table 10: Landslide in different classes of LULC

LULC classes	No. of pixel	Area (%)	No. of landslide	No. of landslide pixel	Landslide area (%)
Forest	2262919	51.284	65	3610	36.33
Grassland	16920	0.383	2	36	0.36
Cropland	1660000	37.62	140	5466	55.01
Builtup Area	350389	7.941	3	58	0.58
Water Bodies	31072	0.704	1	15	0.15
Bare Land	67459	1.529	5	723	7.28
River Bed	23798	0.539	2	28	0.28
Total	4413024	100	218	9936	100

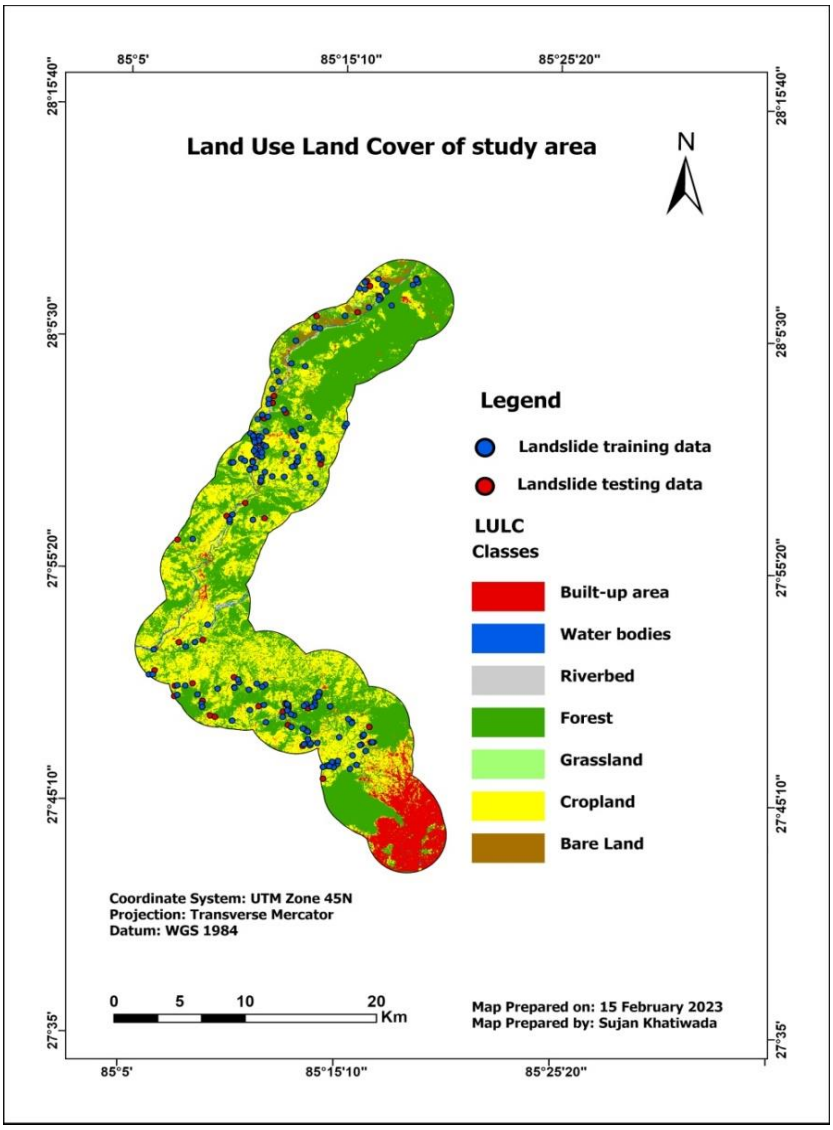

Map 10: Land Use Land Cover of study area

Accuracy Assessment

Table 11 shows the error matrix table for supervised classification. The outcomes demonstrate a total accuracy of 89.20% and a total kappa accuracy of 84.02%. The matrix results revealed that the forest class had the greatest producer accuracy, standing at 93.52%, while water bodies had the second-highest producer accuracy, with 92.86%. However, the producer accuracy for grassland was the lowest at 69.23%, compared to the accuracy results of the other classes. Additionally, the user's accuracy for water bodies was found to be the highest with a 100% accuracy result, followed by built-up areas with

90.91% accuracy.

Table 11: Error matrix: accuracy assessment for Supervise classification of LULC classes

Classified Data	Forest	Grass land	Crop land	Built-up area	Water bodies	Bare land	River bed	Total	U_Accuracy	Kappa
Forest	202	1	19	1	1	1	1	226	89.38	0
Grassland	0	9	2	0	0	1	0	12	75.00	0
Cropland	12	1	149	3	0	0	1	166	89.76	0
Built-up area	2	0	2	40	0	0	0	44	90.91	0
Water bodies	0	0	0	0	13	0	0	13	100.00	0
Bareland	0	2	2	0	0	18	0	22	81.82	0
Riverbed	0	0	2	0	0	0	15	17	88.23	0
Total	216	13	176	44	14	20	17	500	0.00	0
P_Accuracy	93.52	69.23	84.66	90.91	92.86	90.00	88.24	0	89.20	0
Kappa	0	0	0	0	0	0	0	0	0	84.02

4.2.8 Geology

Geology is another important factor that directly influences the occurrence of landslides. The impact of geology on landslides is widely acknowledged, as differences in the durability and permeability of rocks and soils caused by lithological and structural variations can lead to such occurrences (Ayalew & Yamagishi, 2005). Landslide events distributions in different geological formation classes are shown in map 11. Table 12

Table 12: Landslides in different geological formation class

Geology classes	No. of landslide	No of landslide pixel	Landslide area (%)
Himal Group	0	0	0
Ghanapokhara Formation	0	0	0
Ranimatta Formation	112	8888	89.45
Ulleri Formation	1	116	1.17
Sangram Formation	0	0	0
Gn	41	244	2.46
Naudanda Formation	0	0	0
Galyang Formation	6	36	0.36
Sh	48	566	5.70
Udayapur Formation	3	10	0.10
Rb	0	0	0
Chandragiri Formation	6	73	0.73
Recent	0	0	0
Tistung Formation	1	3	0.03
Sopyang Formation	0	0	0
Upper Siwalik	0	0	0
Total	218	9936	100

shows that almost 90% landslide pixels were found in Ranimatta formation class from 112 landslides events. Moreover, table 12 also shows that smaller landslides were observed in Gn and Sh class of geology because only 244 and 566 landslides pixels were found there from 41 and 48 landslides respectively.

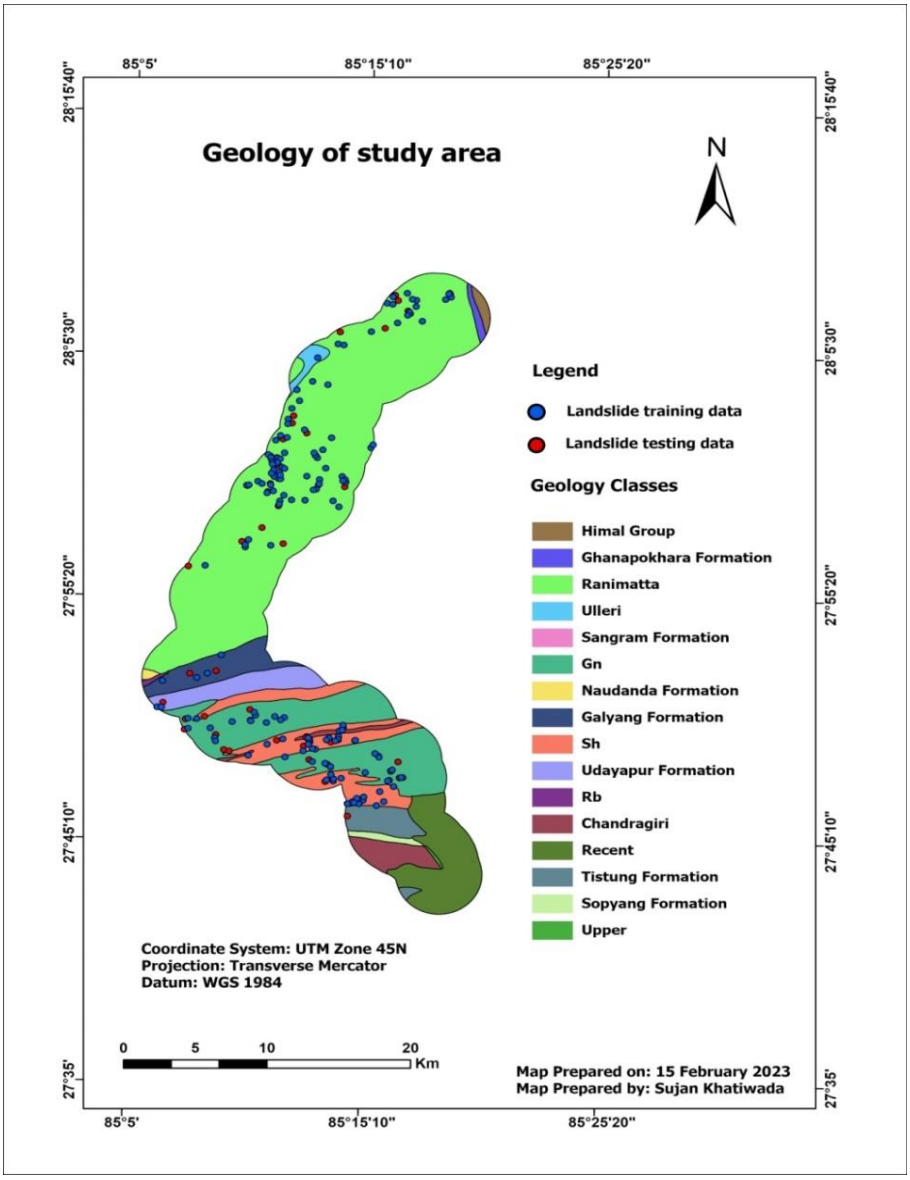

Map 11: Geology of study area

4.2.9 Distance to drainage

Distance to drainage is another geomorphology-related causative factor for landslides. The level of saturation of the slope's material governs a slope's stability. Map 12 displays

the occurrence of landslides at different distances from drainage networks, indicating that the maximum landslide areas were concentrated closer to the drainage network. According to Table 13, there were 89 landslides that took place within 100 meters of the drainage networks. Within a distance of less than 50 meters from the stream network, 24% of the landslide areas were recorded, while the least amount of landslide area (6.61%) was found within a distance class of 200-250 meters from the stream network. Additionally, approximately 63% of landslide areas were found to occur below a distance of 200 meters from drainage networks, while only 10 landslides took place at a distance of 300-350 meters from the drainage network.

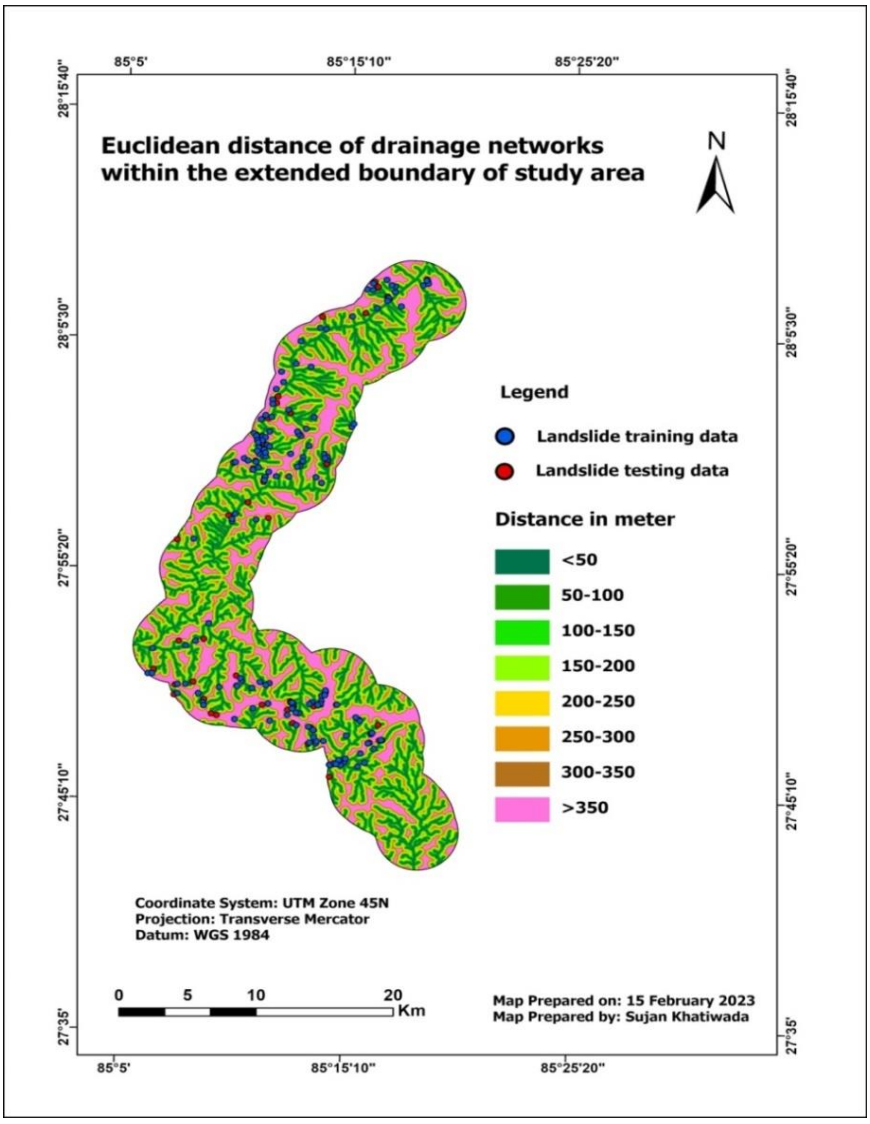

Map 12: Euclidean distance of drainage network

Table 13: Landslide at different distance from drainage networks

Drainage distance classes	No. of landslide	No of landslide pixel	Landslide pixel (%)
<50	42	2300	23.15
50-100	47	1894	19.06
100-150	29	1442	14.51
150-200	28	1145	11.52
200-250	14	665	6.69
250-300	20	671	6.75
300-350	10	612	6.16
>350	28	1207	12.15
Total	218	9936	100

4.2.10 Distance to road networks

The road network can have a significant impact on the occurrence of landslides. Building roads on unstable terrain can increase the risk of landslides. Map 13 displays the distribution of landslide events at different distance classes from the road network. It was found that 43.44% of landslide pixels from only 20 landslides took place at a distance of above 500m from the road network. Additionally, Table 14 shows that only 2335 landslide pixels from 156 landslides were found below 100 meters from the road network.

Table 14: Landslide at different distance from road network

Road distance classes (m)	No. of landslide	No of landslide pixel	Landslide area (%)
Below 100	156	2335	23.50
100-200	20	1258	12.66
200-300	14	1045	10.52
300-400	5	665	6.69
400-500	3	317	3.19
above 500	20	4316	43.44
Total	218	9936	100

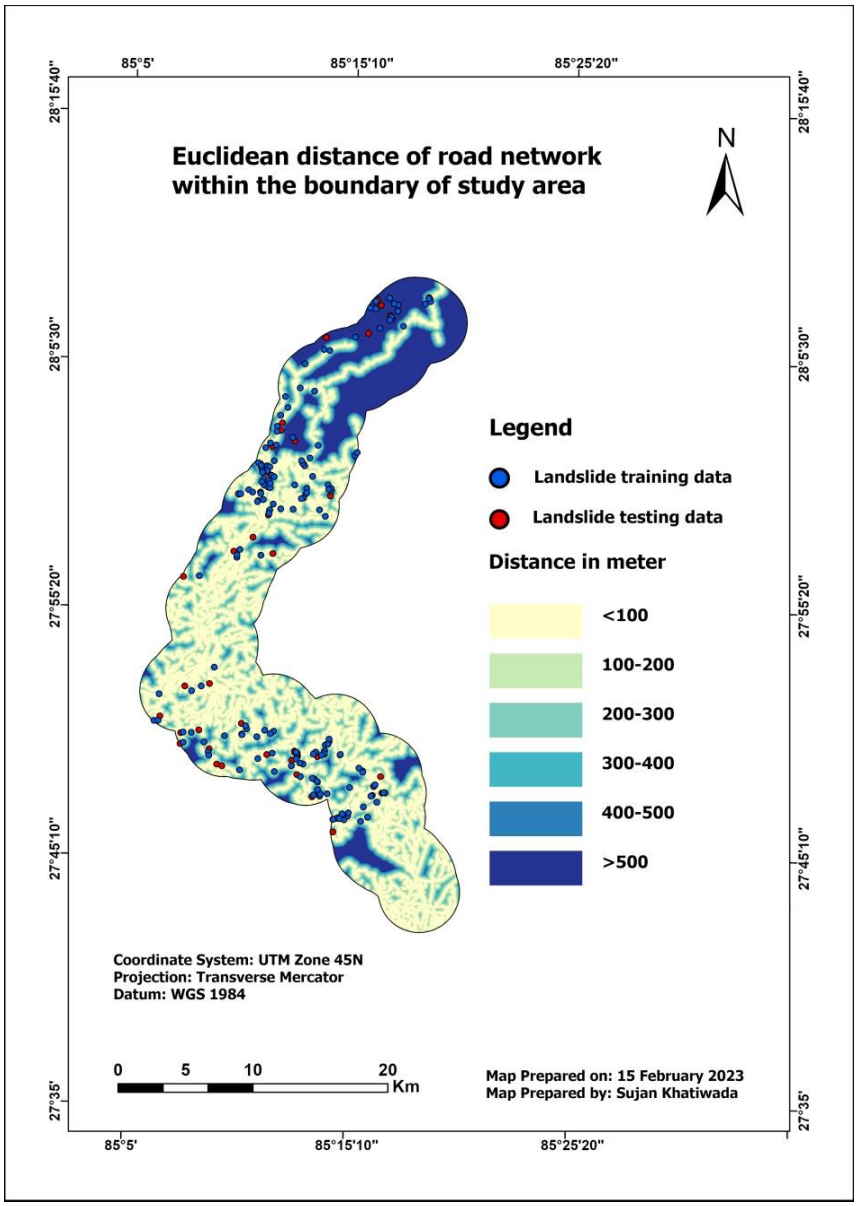

Map 13: Euclidean distance of road networks

4.3 Landslide Susceptibility Mapping

In this study Landslide Susceptibility Index Map was created by using FR and AHP methods.

4.3.1 Frequency Ratio Model

Relative frequency is the ratio of the landslide area that occurred in past in different classes of causative factors to area of causative factor's class. The fundamental principle

of FR is that future landslides are likely to occur if the conditions are identical to those that caused past landslides. The FR value for all factor's classes are tabulated below. Integer values for FR for each factor were calculated to make the reclassification causative factor easy based on the integer value.

Table 15: Frequency ratio of causative factors

Causative Factors	Class	No. of pixels in class	Pixels area (%)	landslides pixels	landslide pixels area (%)	FR	Integer
Slope							
1	<10°	646666	14.654	20	0.298	0.020	2
2	10°-20°	893455	20.246	283	4.215	0.208	20
3	20°-30°	1504800	34.099	2277	33.914	0.995	99
4	30°-40°	961919	21.797	2922	43.521	1.997	199
5	40°-50°	318630	7.220	1065	15.862	2.197	219
6	>50°	87554	1.984	147	2.189	1.104	110
	Total	4413024	100.000	6714	100.000	6.520	652
Aspect							
1	Flat	52031	1.179	3	0.045	0.038	3
2	North	534706	12.117	57	0.849	0.070	7
3	Northeast	452842	10.261	142	2.115	0.206	20
4	East	471079	10.675	707	10.530	0.986	98
5	Southeast	618914	14.025	1837	27.361	1.951	195
6	South	558197	12.649	1457	21.701	1.716	171
7	Southwest	494978	11.216	1656	24.665	2.199	219
8	West	570677	12.932	682	10.158	0.786	78
9	Northwest	659600	14.947	173	2.577	0.172	17
	Total	4413024	100.000	6714	100.000	8.124	812
LULC							
1	Forest	2262919	51.284	2152	32.052	0.625	62
2	Grassland	16920	0.383	23	0.343	0.893	89
3	Cropland	1660000	37.620	4049	60.307	1.603	160
4	Builtup Area	350389	7.941	44	0.655	0.083	8
5	Water Bodies	31072	0.704	6	0.089	0.127	12
6	Bare Land	67459	1.529	429	6.390	4.180	417
7	River Bed	23798	0.539	11	0.164	0.304	30
	Total	4413024	100.000	6714	100.000	7.814	781
Geology							
1	Himal Group	20201	0.458	0	0.000	0.000	0
2	Ghanapokhara Formation	18668	0.423	0	0.000	0.000	0
3	Ranimatta Formation	2248698	50.956	5892	87.757	1.722	172
4	Ulleri Formation	34207	0.775	116	1.728	2.229	222
5	Sangram	204	0.005	0	0.000	0.000	0

	Formation						
6	Gn	747678	16.943	179	2.666	0.157	15
7	Naudanda Formation	6739	0.153	0	0.000	0.000	0
8	Galyang Formation	175337	3.973	15	0.223	0.056	5
9	Sh	387521	8.781	457	6.807	0.775	77
10	Udayapur Formation	168416	3.816	7	0.104	0.027	2
11	Rb	5398	0.122	0	0.000	0.000	0
12	Chandragiri Formation	127321	2.885	48	0.715	0.248	24
13	Recent	334045	7.570	0	0.000	0.000	0
14	Tistung Formation	110501	2.504	0	0.000	0.000	0
15	Sopyang Formation	24153	0.547	0	0.000	0.000	0
16	Upper Siwalik	3937	0.089	0	0.000	0.000	0
	Total	4413024	100.000	6714	100.000	5.215	521
Precipitation							
1	845-1000mm	34419	0.780	0	0.000	0.000	0
2	1000-1200mm	108339	2.455	0	0.000	0.000	0
3	1200-1400mm	329066	7.457	445	6.628	0.889	88
4	1400-1600mm	733939	16.631	4121	61.379	3.691	369
5	1600-1800mm	1494772	33.872	1151	17.143	0.506	50
6	1800-2000mm	1166340	26.429	915	13.628	0.516	51
7	2000-2214mm	546149	12.376	82	1.221	0.099	9
	Total	4413024	100.000	6714	100.000	5.700	569
Distance to drainage networks							
1	<50m	698846	15.836	1673	24.918	1.574	157
2	50-100m	592849	13.434	1226	18.260	1.359	135
3	100-150m	543204	12.309	799	11.901	0.967	96
4	150-200m	488614	11.072	555	8.266	0.747	74
5	200-250m	432959	9.811	444	6.613	0.674	67
6	250-300m	378048	8.567	463	6.896	0.805	80
7	300-350m	321821	7.293	483	7.194	0.986	98
8	>350m	956683	21.679	1071	15.952	0.736	73
	Total	4413024	100.000	6714	100.000	7.848	784
Distance to road networks							
1	<100m	1803873	40.876	1988	29.610	0.724	72
2	100-200m	886253	20.083	1062	15.818	0.788	78
3	200-300m	499506	11.319	829	12.347	1.091	109
4	300-400m	300524	6.810	608	9.056	1.330	132
5	400-500m	177775	4.028	125	1.862	0.462	46
6	>500m	745093	16.884	2102	31.308	1.854	185

	Total	4413024	100.000	6714	100.000	6.249	624
Elevation							
1	<1000m	1361204	30.845	1155	17.203	0.558	55
2	1000-1500m	1512383	34.271	2228	33.184	0.968	96
3	1500-2000m	926081	20.985	2851	42.464	2.023	202
4	2000-2500m	344964	7.817	480	7.149	0.915	91
5	2500-3000m	173848	3.939	0	0.000	0.000	0
6	>3000m	94544	2.142	0	0.000	0.000	0
	Total	4413024	100.000	6714	100.000	4.464	446
TWI							
1	1.01 - 4.69	1442364	32.684	2083	31.025	0.949	94
2	4.69 - 6.57	2013234	45.620	2897	43.149	0.946	94
3	6.57 - 9.40	710137	16.092	1398	20.822	1.294	129
4	9.40 - 14.40	217477	4.928	335	4.990	1.012	101
5	14.40 - 25.05	29812	0.676	1	0.015	0.022	2
	Total	4413024	100.000	6714	100.000	4.224	422
Curvature profile							
1	-23.20 To -2.00	65784	1.491	109	1.623	1.089	108
2	-2.00 To -0.50	1141540	25.868	1572	23.414	0.905	90
3	-0.50 To 0.35	1771315	40.138	2564	38.189	0.951	95
4	0.35 To 1.64	1304098	29.551	2119	31.561	1.068	106
5	1.64 To 31.41	130287	2.952	350	5.213	1.766	176
	Total	4413024	100.000	6714	100.000	5.779	577

Table 15 displays the FR values for each class of causative factors. The probability of landslides taking place is linked directly to the FR value, and a greater value suggests a more robust correlation between the factors leading to landslides and their occurrence. All causative factors were reclassified based on the FR value. In this case, to simplify the reclassification process, RF values were converted to integers Table 15 displays the highest FR value in the slope class of 40 to 50 degrees, which indicates a strong correlation between this slope class and landslide occurrence. Similarly, the southwest aspect is highly susceptible to landslides, followed by the southeast and south aspects, with their FR values being 2.19, 1.95, and 1.71, respectively. Additionally, the Ulleri formation of geology shows a strong correlation with landslides occurrence, as its FR is found to be high (2.22) compared to other classes. Table 15 also reveals that bare land has the strongest correlation to landslides, with an FR of 4.18. The likelihood of landslides

is significantly higher in places with an average annual rainfall of 1400mm to 1600mm, and the highest FR value is observed in this particular category. Conversely, there is less risk of landslides in an area receiving a mean annual precipitation below 1200mm (Table 15). Higher FR values for an area closer to the stream networks indicate that these areas are in danger of landslides. It was found that there is an inverse relationship between FR values and distance to stream network classes from <50m up to 200-250m (Table 15). Similarly, Table 15 shows that areas above 500m from networks are highly susceptible to landslides having the highest FR value about 1.85. Areas located in an elevation between 1500-2000m show a strong correlation to landslides occurrence, as this elevation class has the highest FR value. Meanwhile, areas above 2500m elevation pose less risk for landslides, as no landslides have occurred in the past (Table 15). The table also shows the highest FR value (1.29) for areas with a TWI between 6.57 and 9.40. This means that areas in this class are highly at risk for landslides. Similarly, regions exhibiting a curvature profile exceeding 1.64 have a high likelihood of experiencing landslides, as the FR value is maximum in this class (Table 15).

4.3.1.1 Landslide Susceptibility Index map from FR

LSI map shows the susceptibility of the research area based on the range of continuous value. Pixels with smaller values are less susceptible while pixels with larger values are highly susceptible to landslides. The classified LSI Map prepared from FR is shown in map 14.

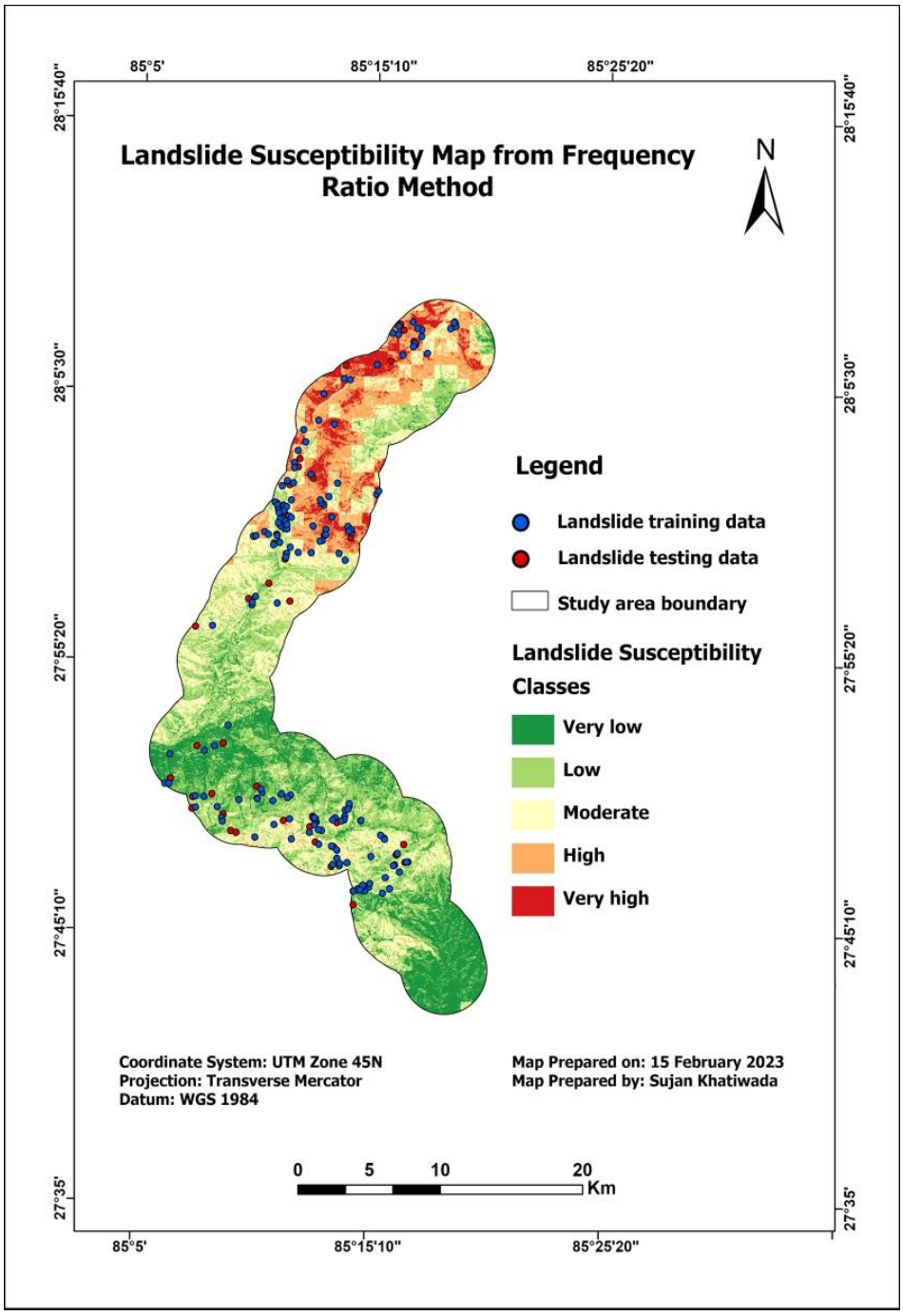

Map 14: Landslide Susceptibility map from Frequency Ratio Method

4.3.2 AHP model

In AHP model, relative value for all factor's classes were calculated based on landslide density from inventory data. Later rating value for each class was obtained by formation of pairwise comparison table by using AHP methods. The pair-wise comparison matrix for causative factors and their respective classes are given in table 16 and 17.

Table 16: The pair-wise comparison matrix, factor weights and consistency ratio

Causative Factors												
		{A}	{B}	{C}	{D}	{E}	{F}	{G}	{H}	{I}	{J}	Weightage
{A}	Slope	1										0.2862
{B}	Lithology	1/2	1									0.2036
{C}	Precipitation	1/3	1/2	1								0.1465
{D}	Distance from stream	1/4	1/3	1/2	1							0.1279
{E}	LULC	1/5	1/4	1/3	1/3	1						0.0746
{F}	Distance from road	1/5	1/4	1/4	1/4	1/2	1					0.0538
{G}	elevation	1/6	1/5	1/4	1/5	1/3	1/2	1				0.0395
{H}	Curvature	1/7	1/6	1/5	1/5	1/4	1/3	1/2	1			0.0259
{I}	TWI	1/7	1/6	1/5	1/6	1/4	1/3	1/3	1/2	1		0.0217
{J}	Aspect	1/9	1/7	1/6	1/6	1/5	1/4	1/3	1	1	1	0.0203
λmax=10.622, CR=0.046												

Table 17: The pair-wise comparison matrix, class weights (rating) and consistency ratio

ASPECT												
		{A}	{B}	{C}	{D}	{E}	{F}	{G}	{H}	{I}	Weight	Integer
{A}	Flat	1									0.0251	2
{B}	North	1	1								0.0251	2
{C}	North east	2	2	1							0.0372	4
{D}	East	4	4	2	1						0.0776	8
{E}	Southeast	7	7	7	5	1					0.3003	30
{F}	South	6	6	6	3	1/2	1				0.1792	18
{G}	Southwest	7	7	7	4	1/2	2	1			0.2376	24
{H}	West	4	4	3	1	1/5	1/3	1/4	1		0.0816	8
{I}	Northwest	2	2	1	1/3	1/7	1/6	1/6	1/3	1	0.0364	4
λmax=9.31, CR=0.027												
LULC												
		{A}	{B}	{C}	{D}	{E}	{F}	{G}			Weight	Integer
{A}	Forest	1									0.2963	30
{B}	Grassland	1/8	1								0.0375	4
{C}	Cropland	3	9	1							0.4528	45
{D}	Builtup	1/8	1	1/9	1						0.0512	5
{E}	Water bodies	1/8	1	1/9	1/2	1					0.0340	3
{F}	Bareland	1/5	3	1/6	3	3	1				0.0952	10
{G}	River bed	1/8	1	1/9	1/3	1	1/3	1			0.0329	3
λmax=7.318, CR=0.0395												
Precipitation												
		{A}	{B}	{C}	{D}	{E}	{F}	{G}			Weight	Integer
{A}	845-1000mm	1									0.0359	4

{B}	1000-1200mm	1	1								0.0359	4
{C}	1200-1400mm	2	2	1							0.0661	7
{D}	1400-1600mm	9	9	6	1						0.4645	46
{E}	1600-1800mm	7	7	4	1/4	1					0.2186	22
{F}	1800-2000mm	5	5	3	1/5	1/2	1				0.1269	12
{G}	2000-2214mm	1	1	1/2	1/8	1/5	1	1			0.0522	5
λmax=7.39155, CR=0.048												
Distance to Drainage Network												
		{A}	{B}	{C}	{D}	{E}	{F}	{G}	{H}		Weight	Integer
{A}	<50m	1									0.3032	30
{B}	50-100m	1/2	1								0.2334	23
{C}	100-150m	1/3	1/3	1							0.1049	10
{D}	150-200m	1/5	1/4	1/2	1						0.0651	7
{E}	200-250m	1/6	1/5	1/3	1/2	1					0.0390	4
{F}	250-300m	1/6	1/5	1/3	1/2	1	1				0.0390	4
{G}	300-350m	1/6	1/5	1/3	1/2	1	1	1			0.0390	4
{H}	>350m	1/2	1/2	2	3	5	5	5	1		0.1765	18
λmax=8.13, CR=0.013												
Distance to Road Network												
		{A}	{B}	{C}	{D}	{E}	{F}				Weight	Integer
{A}	<100m	1									0.3204	32
{B}	100-200m	1/3	1								0.1464	15
{C}	200-300m	1/5	1/2	1							0.0986	10
{D}	300-400m	1/6	1/3	1/2	1						0.0630	6
{E}	400-500m	1/9	1/7	1/6	1/4	1					0.0240	2
{F}	>500m	2	3	3	4	9	1				0.3475	35
λmax=6.306, CR=0.049												
Altitude												
		{A}	{B}	{C}	{D}	{E}	{F}				Weight	Integer
{A}	<1000m	1									0.1590	16
{B}	1000-1500m	3	1								0.2800	28
{C}	1500-2000m	5	2	1							0.4292	43
{D}	2000-2500m	1/3	1/4	1/5	1						0.0635	6
{E}	2500-3000m	1/7	1/8	1/9	1/3	1					0.0308	3
{F}	>3000m	1/7	1/8	1/9	1	1	1				0.0375	4
λmax=6.32, CR=0.05												
SLOPE												
		{A}	{B}	{C}	{D}	{E}	{F}				Weight	Integer
{A}	0-10°	1									0.0372	4
{B}	10-20°	3	1								0.0755	7
{C}	20-30°	6	5	1							0.2901	29
{D}	30-40°	7	6	2	1						0.3954	40

{E}	40-50°	4	3	1/3	1/3	1					0.1472	15
{F}	>50°	2	1/2	1/5	1/6	1/3	1				0.0547	5
λmax=6.22, CR=0.03												
curvature												
		{A}	{B}	{C}	{D}	{E}					Weight	Integer
{A}	-23.2051 To -2.0007	1									0.0400	4
{B}	-2.0007 To -0.5013	5	1								0.1818	18
{C}	-0.5013 To 0.3555	7	3	1							0.4298	43
{D}	0.3555 To 1.6404	6	2	1/2	1						0.2786	28
{E}	1.6404 To 31.41245	3	1/4	1/6	1/5	1					0.0698	7
λmax=5.190857, CR=0.04237												
TWI												
		{A}	{B}	{C}	{D}	{E}					Weight	Integer
{A}	1.0195 - 4.6949	1									0.276	28
{B}	4.6949 - 6.5797	2	1								0.4365	43
{C}	6.5797 - 9.4069	1/2	1/3	1							0.1864	19
{D}	9.4069 - 14.4017	1/5	1/6	1/4	1						0.0616	6
{E}	14.4017 - 25.0509	1/6	1/8	1/6	1/2	1					0.0395	4
λmax=5.115108, CR=0.02559												

GEOLOGY																		
		{A}	{B}	{C}	{D}	{E}	{F}	{G}	{H}	{I}	{J}	{K}	{L}	{M}	{N}	{O}	{P}	Weight	Integer
{A}	Himal Group	1																0.0328	3
{B}	Ghanapokhara Formation	1	1															0.0374	4
{C}	Ranimatta Formation	9	9	1														0.3413	34
{D}	Ulleri Formation	2	2	1/8	1													0.0592	6
{E}	Sangram Formation	1	1	1/8	1/2	1												0.0300	3
{F}	Gn	2	1	1/8	1	2	1											0.0585	6
{G}	Naudanda Formation	1	1/2	1/9	1/2	1	1/2	1										0.0326	3
{H}	Galyang Formation	2	2	1/8	1	2	1/2	2	1									0.0478	5
{I}	Sh	3	3	1/6	3	3	3	3	3	1								0.1096	11
{J}	Udayapur Formation	2	2	1/8	1/2	2	1	2	1	1/3	1							0.0535	5
{K}	Rb	1/2	1	1/9	1/2	1	1/2	1	1/2	1/3	1/2	1						0.0288	3
{L}	Chandragiri Formation	1	1/2	1/8	1/2	2	1/2	1/2	1	1/3	1	2	1					0.0434	5
{M}	Recent	1	1	1/9	1	1	1/2	1	1	1/3	1/2	1	1/2	1				0.0330	3
{N}	Tistung Formation	1	1	1/9	1/2	1	1/2	1	1/2	1/3	1/2	1	1/2	1	1			0.0298	3
{O}	Sopyang Formation	1	1	1/9	1/2	1	1/2	1	1	1/3	1/2	1	1/2	1	1	1		0.0312	3
{P}	Upper Siwalik	1	1	1/9	1/2	1	1/2	1	1	1/3	1/2	1	1/2	1	1	1	1	0.0312	3
λmax=16.5483, CR=0.0228																			

The table above (Table 16) shows that the highest weightage value (0.286) was assigned to slope, followed by weightage values of 0.203 and 0.146 to geology and precipitation, respectively. The least weightage value (0.0203) was assigned to aspect. Similarly, Table 17 shows that the highest weightage value (0.341) was given to the Ranimatta formation class of geology, followed by weightage values of 0.109 and 0.05 to the Sh and Gn classes of geology. Landslide areas and frequency of landslides are higher in these areas. Additionally, Table 17 shows that the southern east aspect is highly susceptible, while flat and northern aspects are less susceptible to landslides, with the highest (0.30) and lowest (0.025) weightage values being assigned to their respective classes.

Likewise, Table 17 shows that cropland is highly susceptible, followed by forest area and bare land. The weightage values of 0.452, 0.296, and 0.092 were assigned to cropland, forest, and bare land, respectively, while less weightage values were assigned to built-up areas, water bodies, river beds, and grassland, indicating that these classes have less contribution to landslides. Table 17 indicates that the precipitation category of 1400-1600mm received the highest weightage value of 0.454, whereas the precipitation below 1000mm received the least weightage value of 0.035. This indicates that areas receiving precipitation in the range of 1400 to 1600mm are highly susceptible to landslides.

Drainage lying within 50m from the drainage network received the maximum weightage value (0.30), whereas those located 200-350m away were given the lowest weightage value (0.03). Table 17 shows that areas above 500m of distance have the maximum weightage value (0.34), followed by weightage value of 0.42 to the area below 100m of distance. The maximum weightage value (0.42) was assigned to the elevation class of 1500-2000, indicating that areas lying in this altitude range are highly susceptible to landslides, while minimum weightage value (0.03) was assigned to the area above 2500m of altitude, indicating that it is less susceptible to landslides.

Similarly, the table shows that the area lying between the slope class of 30-40 degrees is highly susceptible to landslides, while the area below 10 degrees of slope class is less susceptible, with the highest (0.39) and lowest weightage (0.03) values being assigned to their respective classes. Moreover, in the case of curvature profile, Table 17 shows that the highest (0.42) and lowest weightage (0.04) values were assigned to the curvature classes of -0.50 to 0.355 and -23.20 to -2.00, respectively. Furthermore, Table 17 shows that the TWI class of 4.69 to 6.57 is highly susceptible to landslides, while the 14.40 to 25.05 TWI class is least susceptible to landslides having weightage value (0.43) and lowest weightage value (0.03) being assigned to their respective classes.

4.3.2.1 Landslide Susceptibility Map from AHP method

Landslide Susceptibility Map from AHP method is shown in Map 15.

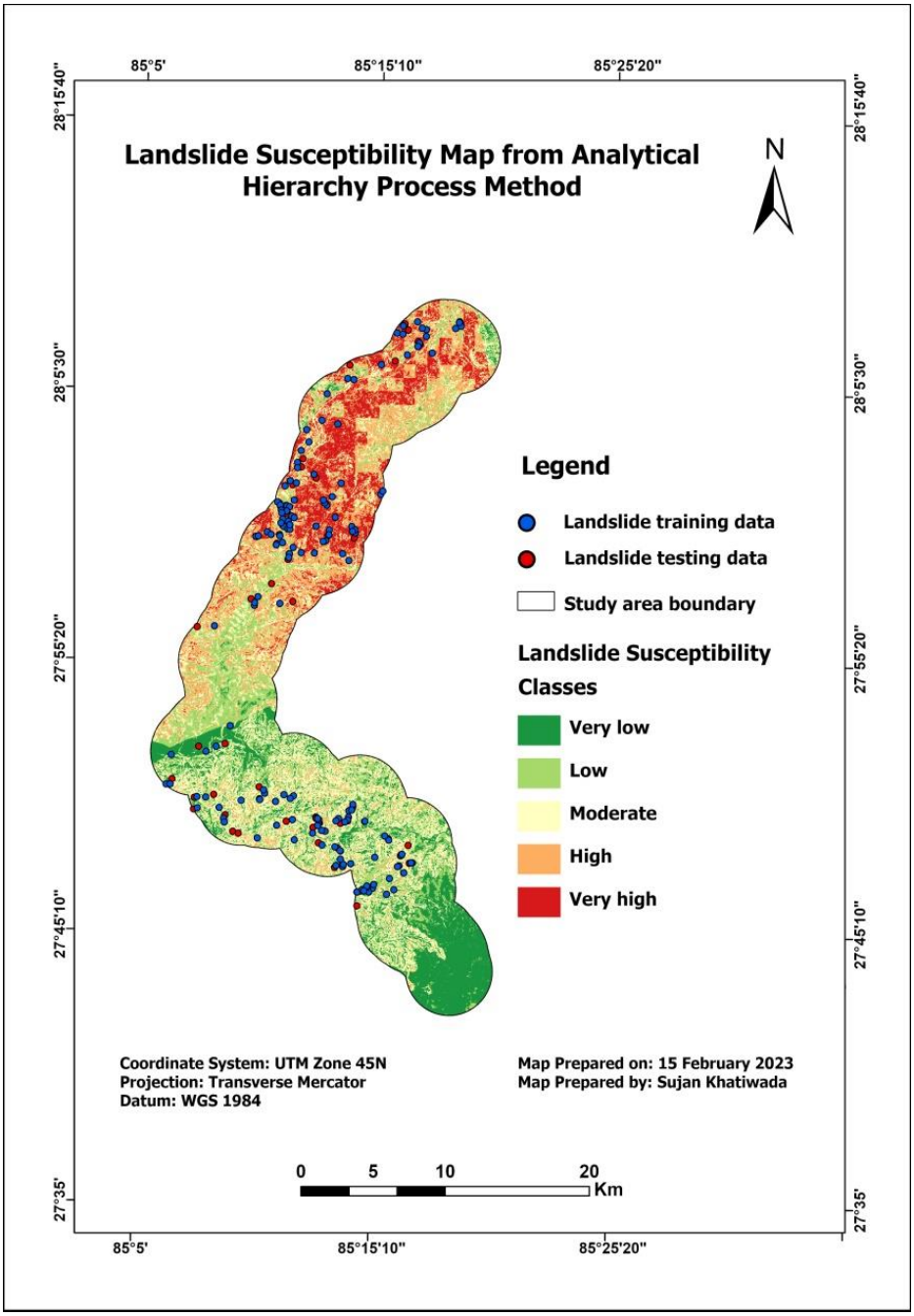

Map 15: Landslide Susceptibility Index Map from AHP Method

4.4 Validation of Landslide Susceptibility Map

Landslide Susceptibility Maps from both methods were verified by using the success rate curve and the prediction rate curve. The success rate curve explains how well the Susceptibility Map is generated based on the existing landslide while the accuracy of the model and predictor variable's ability to forecast the landslide is explained by the

prediction rate. The success rate curve and prediction rate curve for LSI map from FR and AHP methods are shown in figure 3 and figure 4.

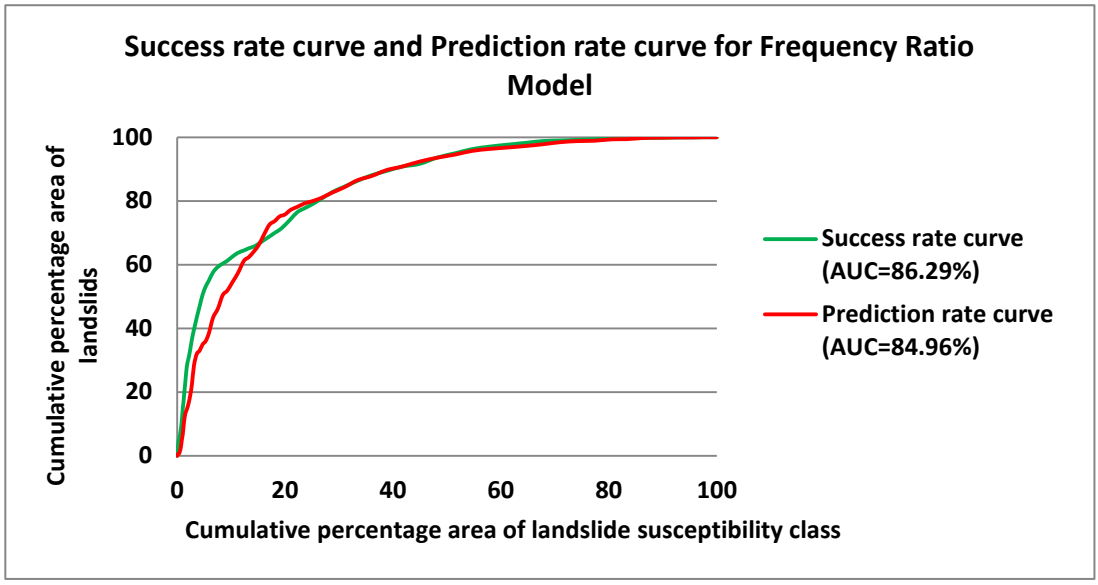

Figure 3: Success rate curve rate for Frequency Ratio Model

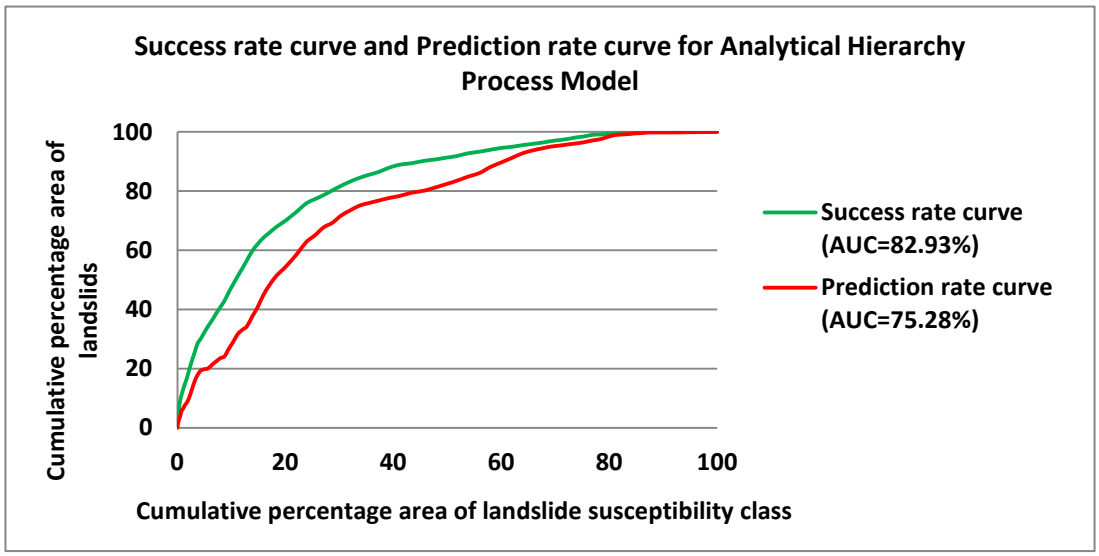

Figure 4: Success rate and prediction rate for AHP model

Figure 3 shows that 89.29% of the region is covered by the success rate curve, while 84.96% is covered by the prediction rate curve. This means that the accuracy for the success rate and prediction rate obtained from the FR model is 89.29% and 84.96%, respectively. Similarly, the accuracy for the success rate curve and prediction rate for the AHP model is 82.93% and 75.28%, respectively (Figure 4).

4.5 Land Use Land Cover in different Susceptibility Classes

4.5.1 LULC in Frequency Ratio Model

It has been obtained that 11.83 Km^2 of the total cropland area lies in very high susceptibility class, as shown in Table 18. Additionally, Table 18 indicates that about 9.58 Km^2, 5.82 Km^2 and 0.03 Km^2 of forest, bare land, and built-up areas, respectively, are also situated in very high susceptibility classes.

Table 18: Area of LULC located in different susceptibility class of LSI map prepared from FR method (Area in square kilometer)

Susceptibility Class	Very Low	Low	Moderate	High	Very High
Built-up Areas	27.9475	5.3883	0.9058	0.7182	0.0397
Water Bodies	1.3092	1.0618	0.302	0.3148	0.1176
River Bed	0.7303	0.8702	0.4454	0.2998	0.0327
Forest	36.92	80.0459	61.514	37.9791	9.5871
Grassland	0.0759	0.3159	0.5617	0.399	0.3337
Cropland	22.1878	56.5852	53.7165	21.4815	11.8338
Bare land	0	0.0075	0.1451	0.7541	5.8284

4.5.2 LULC in Analytical Hierarchy Process Model

Table 19 reveals that about 30 km^2 of the forest areas are situated in very high susceptibility class followed by 23 km^2 of cropland and 0.29 km^2 of built up areas.

Table 19: Area of LULC located in different susceptibility class of LSI map prepared from AHP method (Area in square kilometer)

Susceptibility Class	Very Low	Low	Moderate	High	Very High
Built-up Areas	30.4348	2.4406	1.3405	0.4934	0.2902
Water Bodies	0.7015	1.6404	0.4087	0.1995	0.1553
River Bed	0.4808	1.1326	0.3657	0.2379	0.1614
Forest	23.5991	48.8201	67.2659	55.6566	30.7044
Grassland	0.2402	0.425	0.5169	0.3226	0.1815
Cropland	17.4104	40.5023	50.5349	34.1393	23.2179
Bare land	0.4714	1.9143	1.9253	1.6976	0.7265

4.6 Comparison of LSI maps

4.6.1 Susceptibility Class, training landslides and testing landslide areas

Area covered by different susceptibility class and training and testing landslides areas in each susceptibility classes are shown in table 20.

Table 20; Comparison table for map obtained from FR and AHP Model

FR Model								
Class number	Reclassified index value	Susceptibility Classes	Number of pixels	Susceptibility classes area (%)	Training Pixels	Training landslide area (%)	Testing pixels	Testing landslide area (%)
1	372 - 770	Very Low	897176	20.33	36	0.54	22	0.68
2	770 - 959	Low	1442748	32.69	448	6.67	208	6.47
3	959 - 1189	Moderate	1175905	26.65	1324	19.72	533	16.58
4	1189 - 1467	High	619465	14.04	1122	16.71	1144	35.59
5	1467 - 2245	Very High	277730	6.29	3784	56.36	1307	40.67
AHP Model								
Class number	Reclassified index value	Susceptibility Classes	Number of pixels	Susceptibility classes area (%)	Training Pixels	Training landslide area (%)	Testing pixels	Testing landslide area (%)
1	5.678 - 14.956	Very Low	738852	16.74	17	0.25	24	0.75
2	14.956 - 19.596	Low	968753	21.95	327	4.87	273	8.49
3	19.596 - 24.106	Moderate	1223579	27.73	700	10.43	505	15.71
4	24.106 - 29.132	High	927469	21.02	1920	28.60	1318	41.01
5	29.132 - 38.541	Very High	554372	12.56	3750	55.85	1094	34.04

It has been found that about 20.33% and 33.58% of the research area are found to be situated in higher susceptibility classes for AHP and FR model respectively (table 20). LSI from AHP model shows that about 13% more areas are in risk of loss in near than that obtained from RF model. Table 20 shows that about 73% and 84% of and of training landslides are found to occur in higher susceptibility classes of FR and AHP model respectively. This means AHP has 11% more landslide area in higher susceptibility class than FR model. Moreover, both the model shows equal percentage (75%) of testing landslides found to occur in higher susceptibility zone making the area very risky for landslide (table 20).

4.6.2 Area coverage by LULC in different susceptibility class

The bar graph in figure 5 compares the results obtained from AHP and FR models. Less the 1 Km^2 of built-up areas are located in very susceptibility classes in both models. 30.70 Km^2 and 9 Km^2 of the forest area are situated inside very high susceptibility zone of AHP and FR model respectively. This means that about 21 Km^2 more forest areas are in high risk of sliding in future as shown by AHP model than FR model. Similarly, figure 5 shows that 23.22 Km^2 and 11.83 Km^2 of the cropland are in very high susceptibility zone of AHP and FR model. This means that AHP has about 12km^2 more areas in high risk of loss in future than FR model. Likewise, figure 5 shows that out of 6.74 Km^2 of the total bare land in the research area, 5.83 Km^2 (86.49%) of the bare land lies in very high susceptibility class of AHP model. While FR shows only 0.37 Km^2 of bare land areas are located in very high susceptibility zone. This shows that the probable loss of bare land in future from FR

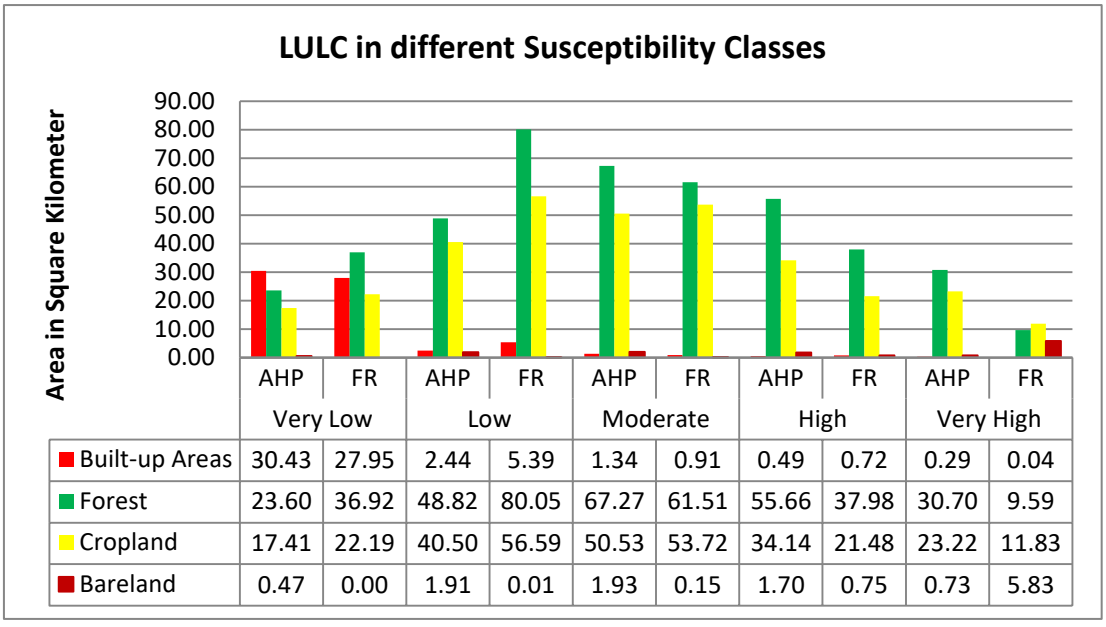

	AHP	FR	AHP	FR	AHP	FR	AHP	FR	AHP	FR
	Very Low		Low		Moderate		High		Very High	
Built-up Areas	30.43	27.95	2.44	5.39	1.34	0.91	0.49	0.72	0.29	0.04
Forest	23.60	36.92	48.82	80.05	67.27	61.51	55.66	37.98	30.70	9.59
Cropland	17.41	22.19	40.50	56.59	50.53	53.72	34.14	21.48	23.22	11.83
Bareland	0.47	0.00	1.91	0.01	1.93	0.15	1.70	0.75	0.73	5.83

Figure 5: Area coverage by LULC in different susceptibility classes

model is extremely high as compare to AHP model.

4.6.3 Accuracy assessment of Models

Accuracy assessment of LSI maps was checked by using AUC curve methods. The AUC for the success rate and prediction rate curve for the FR model were found to be 86.29%

and 84.29%, respectively. While it was found to be 82.93% and 75.28% respectively for AHP model. This demonstrates that AUC for the FR model is greater than AHP model for both the success rate curve and prediction rate curve. This means that FR model is about 4% more accurate for building the LSI model than AHP while prediction rate is about 9% higher than that of AHP.

Chapter-5: Discussions

The present study involved carrying out a landslide inventory through direct site visits, with the aim of assessing the frequency and distribution of landslides pixels across different classes of landslide causative factors. The results revealed that the highest landslide events (168) and landslide pixels (75.29%) occurred within a slope between 20 to 40 degrees, indicating that this class is highly susceptible to landslides. Additionally, slopes facing the southeast aspect exhibited the maximum landslide events (41) and landslide pixels (34.30%), suggesting that this aspect is highly prone to landslides. In terms of geology, the maximum landslides events and landslide pixels were detected in the Ranimatta formation class of geology, indicating that this class is highly risk to landslides. Moreover, the presence of over 50% of landslides from 140 total landslides in cropland highlights the contribution of agricultural practices to landslides in a research area, likely due to inadequate agricultural management systems. The study also revealed that smaller but more frequent landslides occurred in areas with an annual precipitation of 1800 to 2000 millimeters, demonstrating that highly precipitated areas are highly prone to frequent landslides. Additionally, the analysis of the road network indicated that areas closer to roads had a higher susceptibility to frequent landslides, with smaller but maximum landslide events (156) observed within 100 meters of the road network. Furthermore, landslide events decreased gradually as the distance from stream network increased from 50 to 100 meters up to 300 to 300 meters, highlighting the higher susceptibility of areas closer to stream networks to landslides. Moreover, the study found that areas lying at an altitude between 1500 and 2000 meters from sea level are highly at risk of sliding, as the maximum number of landslides (82) and landslide pixels (40.08%) were observed in this elevation class. Similarly, areas with a topographic wetness index (TWI) ranging from 4.69 to 6.57 were found to be at high risk of landslide in the future, with the maximum landslide events (114) recorded in this class, which had 43.89% of landslide pixels. Additionally, 68.4% of landslide pixels from 163 landslides were found in the curvature profile class

between -0.50 to 1.64, highlighting the high susceptibility of areas in this profile range to landslides.

Moreover, the contributions of each factor's classes were assessed based on FR value and weightage value assigned to causative factor's classes. Factor classes having higher weightage value and FR value greater than one are highly susceptible to landslides. This study shows that the area lying between 30-40 degrees and 40-50 degrees of slope are highly susceptible to landslides as the weightage and FR value of these classes are very high. The justification for this is that when the slope gradient increases, the soil's shear stress also rises, rendering it more prone to failure (Saha et al., 2002). Higher FR values of 2.19, 1.95, and 1.71, and higher weightage values of 0.23, 0.3, and 0.17 were found in the southwest, southeast, and southern aspects of the research area. This shows that the slope facing the southeast, southwest, and southern aspects of the research area are highly susceptible to landslides as these sites are frequently exposed to sunlight, and the monsoon increases the likelihood of landslides in these aspects (Thapa & Bhandari, 2019). The study of Shrestha et al. (2021) had also shown the similar results, where the slope facing the southeast aspect was highly susceptible, followed by the south and southwest, having the FR values of 1.97, 1.78, and 1.11, respectively. Moreover, similar results were also obtained from the study of Veerappan et al. (2017) conducted in the part of National Highway, Uttarakhanda, India. This study shows that bare land and crop land have a strong correlation with landslides. The area lying in these classes is highly at risk for landslides because the FR value for bare land and crop land was found to be 4.18 and 1.6, respectively, while the weightage value for cropland alone was 0.45. Research from Veerappan et al. (2017) and Hepdeniz (2020) also showed similar results, as the FR value for bare land was found to be higher, followed by cropland. Similarly, in the case of stream network, the FR and weightage value were found to be higher in the area which is closer to the stream network. This means that the region closer to the stream networks is highly susceptible to landslides. Kayastha et al. (2013) also found similar results. Moreover,

geology is also crucial factor for landslides. In this research, Ulleri Formation and Ranimatta Formation class of geology are highly susceptible to landslides because the maximum FR value (2.22) was found in the Ulleri Formation class, while the maximum weightage (0.341) was assigned to the Ranimatta formation class. Similarly, the TWI class having a value ranging from 4.694 to 6.579 and 6.579 to 9.406 were found to be highly prone to landslides, as this class has the maximum FR value (1.294) and weightage value (0.436). A higher TWI value indicates a larger likelihood of surface water accumulation, which is typically present at lower slopes. The curvature profile class ranging from -0.5013 to 0.355 and 1.6404 to 31.41 was found to be highly susceptible, as the highest FR value (1.765) and weightage value (0.429) were found in respective classes. Similarly, it has been founded that concave surfaces are highly susceptible to landslide incidents due to the justification that rainfall water flows from a convex to concave surface and accumulates in a concave surface (Dahal, 2017). Additionally, both models employed in the study indicate that areas situated above 500m from the road networks are vulnerable to landslides, however, based on the frequency of landslide events, the areas closer to road networks are more susceptible, as 107 landslides (training) were recorded below 100m from the road network. The occurrence of frequent, smaller landslides closer to the highway is attributed to the penetration of a large volume of water from the slope cutting cracks, which induces oversaturation of water content in the soil, ultimately leading to the sliding of the sloppy land. Moreover, the study reveals that areas closer to stream networks are also prone to landslides, as both models show higher weightage and FR values. The continuous erosion of slopes or the saturation of the lower parts of the materials till the water level rises may adversely affect the slope stability (Dai et al., 2002; Saha et al., 2002). The study further confirms that areas situated in an altitude range of 1500 to 2000m receiving an annual mean precipitation of 1400-1600mm are highly susceptible to landslides because the FR value and weightage value are found to be high in these classes.

Based on weightage of factors/factor's classes and FR values LSI map were developed

for landslide susceptibility assessment. FR model shows 14.04% and 6.29% of the research area lie in high and very high susceptibility classes. Similarly, AHP models reveals 21.02% and 12.56% of research area situated inside high and very high susceptible classes. LSI from AHP reveals about 13% more areas lie in higher susceptibility classes. The landslide susceptibility index maps were validated by comparing the existing landslide data and susceptibility analysis results. 70% (153) and 30% (65) landslides were used to generate success rate and prediction rate curves, respectively. AUC values were calculated for accuracy assessment of both susceptibility maps. The AUC values ranged from 0.50 to 1.00, with 0.50 to 0.60 indicating fail, 0.60 to 0.70 indicating poor, 0.70 to 0.80 indicating fair, 0.80 to 0.90 indicating good, and 0.90 to 1.00 indicating excellent accuracy. LSI map from FR model showed that 86.29% and 84.96% of the area lie under success rate and prediction rate curves, respectively. For the AHP model, it was found that 82.93% and 75.25% of the area lie under success rate and prediction rate curves, respectively. The FR model was found to be about 3% more accurate than the AHP model. Moreover, the FR model could predict landslides more precisely than the AHP model, with a 10% higher accuracy. Comparative studies conducted by Panchal and Shrivastava (2021) in Shimla, India have also shown that the FR model is more suitable for landslide susceptibility analysis. The LSI map from the FR model showed that more than 11 Km^2, 9 Km^2, and 5 Km^2 of cropland and forest area are at high risk of loss because they are located in very high susceptible areas.

Pros and Cons of AHP and FR models

AHP is a decision-making tool that allows for the consideration of multiple criteria and alternatives, resulting in a comprehensive evaluation that incorporates various factors and perspectives (Saaty, 2008). This technique provides a structured approach to decision-making, which can ensure that evaluations are consistent and reliable. Furthermore, AHP enables the weighting of criteria depend on their relative importance, allowing for the prioritization of important factors in the decision-making process. AHP also allows for the

incorporation of expert opinion, providing valuable insights and perspectives to the evaluation process (Saaty, 2008). Analytical Hierarchy Process (AHP) can be a complex technique that demands expertise to be used effectively and efficiently (Saaty, 2008). Novice users may face difficulty in understanding and implementing this technique due to its complexity. Additionally, AHP is vulnerable to subjectivity since the weighting of criteria and judgments made during the evaluation process are subjective, which can result in potential bias (Saaty, 2008). Furthermore, the technique requires the availability of data on multiple criteria, which may not always be obtainable or may be challenging to collect (Saaty, 2008). AHP is also sensitive to the inputs used, which implies that small modifications in input may lead to significant changes in output, thereby making the technique less robust and reliable (Saaty, 2008).

Similarly, the FR method is simple and easy to apply, requiring readily available data. This method can identify the most influential factors for landslide occurrence by analyzing their frequency distribution and relationship with landslide events. It is applicable for large areas as it uses statistical analysis of past landslide events to identify areas prone to landslides. But this method is biased towards areas with past landslide events, and may not be accurate in areas without such events. The accuracy of the FR method is limited due to its reliance on past landslide events and the availability of reliable data. The FR method is a statistical approach that does not take into account the physical processes that lead to landslide occurrence. Therefore, the resulting susceptibility map may not accurately reflect the actual landslide hazard in an area. The FR method assumes that the influence of conditioning factors on landslide occurrence is consistent across the entire study area, which may not be accurate in reality.

Chapter-6: Conclusion

In the present study, LSI map was prepared from two methods for comparative study. Ten causative factors were considered for developing LSI map. Slope, aspects, curvature profile, TWI, elevation, distance to drainage network, distance to road networks, geology, precipitation and LULC. In the present point landslide point inventory was performed by directly visiting the site and polygon inventory map was mapped later by using Google Earth. Landslide inventory data was then divided into training (70%) and testing landslides (30%). Landslide density and frequency for each class of landslide causative factors were assessed. Frequency Ratio value and weightage value for each class of causative factors were calculated for evaluating the relation between the landslide and its causative factor classes. Finally, LSI map was prepared and was categorized into five classes: very low, low, moderate, high and very high. The LSI map prepared from frequency shown 14.04% and 6.09% of the total studied areas lie in high and very high susceptibility classes. Similarly, LSI map from AHP model revealed 21.02% and 12.56% area lie in high and very high susceptibility class. Both the models were evaluated by using ROC curve. Similarly, 9.5 and 11.8km^2 of forest and cropland were found to be situate in high susceptible zone of FR model while it 30.7 Km^2 and 23.2 Km^2 square kilometer for AHP model. The prediction rate and success rate of FR model were 84.95% and 86.29% while it was 75.28% and 82.93% for AHP model. This study has shown that FR model is better than AHP model for predicting the landslides that might occur in future based on past condition of past landslides.

LSI map from this study can be a valuable tool in transportation and urban planning to identify areas that are at risk for landslides and to inform decision-making related to infrastructure development and maintenance. In transportation, landslide susceptibility mapping can help identify potential risks to transportation infrastructure, including roads, railways, and bridges, and inform decisions about infrastructure design and maintenance.

For example, the mapping can identify areas that are prone to landslides and guide decisions about the use of mitigation measures such as slope stabilization or retaining walls to protect infrastructure. In urban planning, landslide susceptibility mapping can guide land use planning decisions in urban areas, identifying areas that are at high risk for landslides and guiding the development of infrastructure and buildings in safer locations. This can help prevent the loss of life and property damage from landslides in urban areas. In both transportation and urban planning, landslide susceptibility mapping can be a critical component of disaster risk reduction and emergency management efforts, helping to identify high-risk areas and inform preparedness and response measures in case of a landslide event.

Chater-7: References

Acharya, G., De Smedt, F., & Long, N. T. (2005). Assessing landslide hazard in GIS: A case study from Rasuwa, Nepal. *Bulletin of Engineering Geology and the Environment*, *65*(1), 99-107. https://doi.org/10.1007/s10064-005-0025-y

Acharya, T. D., & Lee, D. H. (2018). Landslide susceptibility mapping using relative frequency and predictor rate along Araniko highway. *KSCE Journal of Civil Engineering*, *23*(2), 763-776. https://doi.org/10.1007/s12205-018-0156-x

Achour, Y., Boumezbeur, A., Hadji, R., Chouabbi, A., Cavaleiro, V., & Bendaoud, E. A. (2017). Landslide susceptibility mapping using analytic hierarchy process and information value methods along a highway road section in Constantine, Algeria. *Arabian Journal of Geosciences*, *10*(8). https://doi.org/10.1007/s12517-017-2980-6

Adhikari, D. P., & Koshimizu, S. (2005). Debris flow disaster at Larcha, upper Bhotekoshi Valley, central Nepal. *The Island Arc*, *14*(4), 410-423. https://doi.org/10.1111/j.1440-1738.2005.00495.x

Agrawal, N., & Dixit, J. (2022). Assessment of landslide susceptibility for Meghalaya (India) using bivariate (frequency ratio and Shannon entropy) and multi-criteria decision analysis (AHP and fuzzy-AHP) models. *All Earth*, *34*(1), 179-201. https://doi.org/10.1080/27669645.2022.2101256

Arsyad, A., & Hamid, W. (2020). Landslide susceptibility mapping along road corridors in West Sulawesi using GIS-AHP models. *IOP Conference Series: Earth and Environmental Science*, *419*(1), 012080. https://doi.org/10.1088/1755-1315/419/1/012080

Asmare, D. (2023). Application and validation of AHP and FR methods for landslide susceptibility mapping around choke mountain, northwestern Ethiopia. *Scientific African*, *19*, e01470. https://doi.org/10.1016/j.sciaf.2022.e01470

Ayalew, L., & Yamagishi, H. (2005). The application of GIS-based logistic regression

for landslide susceptibility mapping in the kakuda-yahiko mountains, central Japan. *Geomorphology*, *65*(1-2), 15-31. https://doi.org/10.1016/j.geomorph.2004.06.010

Beven, K., Kirkby, M. (1979). “A physically based, variable contributing area model of basin hydrology". Hydrological Science Bulletin. 24 (1): 43–69. doi: 10.1080/02626667909491834

Central Bureau of Statistics, Nepal. (2021). National population and housing census 2078 - preliminary results. https://cbs.gov.np/wp-content/uploads/2021/08/National-Population-and-Housing-Census-20112078_Preliminary-Results.pdf

Dahal, R. K. (2013). Regional-scale landslide activity and landslide susceptibility zonation in the Nepal Himalaya. Environmental Earth Sciences, 71(12), 5145-5164. https://doi.org/10.1007/s12665-013-2917-7

Dahal, R. K. (2015). Earthquake-induced slope failure susceptibility in eastern Nepal. *Journal of Nepal Geological Society*, *49*(1), 49-56. https://doi.org/10.3126/jngs.v49i1.23141

Dahal, R. K. (2017). Landslide hazard mapping in GIS. *Journal of Nepal Geological Society*, *53*, 63-91. https://doi.org/10.3126/jngs.v53i0.23808

Dahal, R. K., Hasegawa, S., Nonomura, A., Yamanaka, M., Dhakal, S., & Paudyal, P. (2008). Predictive modelling of rainfall-induced landslide hazard in the lesser Himalaya of Nepal based on weights-of-evidence. *Geomorphology*, *102*(3-4), 496-510. https://doi.org/10.1016/j.geomorph.2008.05.041

Dai, F., & Lee, C. (2002). Landslide characteristics and slope instability modeling using GIS, Lantau island, Hong Kong. Geomorphology, 42(3-4), 213-228. https://doi.org/10.1016/s0169-555x(01)00087-3

Dai, F., Lee, C., & Ngai, Y. (2002). Landslide risk assessment and management: An overview. *Engineering Geology*, *64*(1), 65-87. https://doi.org/10.1016/s0013-7952(01)00093-x

Demir, G., Aytekin, M., Akgün, A., İkizler, S. B., & Tatar, O. (2012). A comparison of landslide susceptibility mapping of the eastern part of the north anatolian fault zone (Turkey) by likelihood-frequency ratio and analytic hierarchy process methods. *Natural Hazards*, *65*(3), 1481-1506. https://doi.org/10.1007/s11069-012-0418-8

Dhital, M. R. (2015). Geology of the Nepal Himalaya: Regional perspective of the classic collided orogen. Springer.

El Jazouli, A., Barakat, A., & Khellouk, R. (2019). GIS-multicriteria evaluation using AHP for landslide susceptibility mapping in Oum ER Rbia high basin (Morocco). *Geoenvironmental Disasters*, *6*(1). https://doi.org/10.1186/s40677-019-0119-7

Erener, A., Mutlu, A., & Sebnem Düzgün, H. (2016). A comparative study for landslide susceptibility mapping using GIS-based multi-criteria decision analysis (MCDA), logistic regression (LR) and association rule mining (ARM). Engineering Geology, 203, 45-55. https://doi.org/10.1016/j.enggeo.2015.09.007

Esaid, O., Abdelkareem, O., Mohamed, H., Elamin, A., Elyas, M., Eltahir, S., Adam, H., Elhaja, M., Rahamtallah Abualgasim, M., Osunmadewa, B., & Elmar, C. (2018). Accuracy Assessment of Land Use Land Cover in Umabdalla Natural Reserved Forest. Vol. 3, 5–9.

Esri. (2021). Resample (Data Management). ArcGIS Pro 2.8. Retrieved from https://pro.arcgis.com/en/pro-app/2.8/tool-reference/data-management/resample.htm (Accessed on January 1, 2023).

Gansser, A. (1964).Geology of the Himalayas. London Wiley Interscience, 289 p.

Glade, T. (2003). Landslide occurrence as a response to land use change: A review of evidence from New Zealand. *CATENA*, *51*(3-4), 297-314. https://doi.org/10.1016/s0341-8162(02)00170-4

Gorsevski, P. V., Gessler, P. E., Foltz, R. B., & Elliot, W. J. (2006). Spatial prediction of landslide hazard using logistic regression and ROC analysis. *Transactions in*

GIS, *10*(3), 395-415. https://doi.org/10.1111/j.1467-9671.2006.01004.x

Guzzetti, F., Cardinali, M., Reichenbach, P., & Carrara, A. (2000). Comparing landslide maps: A case study in the upper Tiber river basin, central Italy. *Environmental Management*, *25*(3), 247-363. https://doi.org/10.1007/s002679910020

Guzzetti, F., Mondini, A. C., Cardinali, M., Fiorucci, F., Santangelo, M., & Chang, K. (2012). Landslide inventory maps: New tools for an old problem. *Earth-Science Reviews*, *112*(1-2), 42-66. https://doi.org/10.1016/j.earscirev.2012.02.001

Hepdeniz, K. (2020). Using the analytic hierarchy process and frequency ratio methods for landslide susceptibility mapping in Isparta-Antalya highway (D-685), Turkey. *Arabian Journal of Geosciences*, *13*(16). https://doi.org/10.1007/s12517-020-05764-2

Joseph, J. G., Ragam, S. P., & Rajitha, R. (2016). A CRITICAL STUDY OF DISASTER AS REFLECTED IN LITERATURE. 6.

Kavzoglu, T., Sahin, E. K., & Colkesen, I. (2013). Landslide susceptibility mapping using GIS-based multi-criteria decision analysis, support vector machines, and logistic regression. *Landslides*, *11*(3), 425-439. https://doi.org/10.1007/s10346-013-0391-7

Kayastha, P., Bijukchhen, S. M., Dhital, M. R., & De Smedt, F. (2013). GIS based landslide susceptibility mapping using a fuzzy logic approach: A case study from ghurmi-dhad Khola area, eastern Nepal. *Journal of the Geological Society of India*, *82*(3), 249-261. https://doi.org/10.1007/s12594-013-0147-y

Khanal, N. R., & Watanabe, T. (2008). Landslide and debris flow in the Himalayas: A case study of the Madi watershed in Nepal. *Himalayan Journal of Sciences*, *2*(4), 180-181. https://doi.org/10.3126/hjs.v2i4.864

Kopecký, M., Macek, M., & Wild, J. (2021). Topographic wetness index calculation guidelines based on measured soil moisture and plant species composition. *Science of The Total Environment*, *757*, 143785. https://doi.org/10.1016/j.scitotenv.2020.143785

Kumar, R., & Anbalagan, R. (2016). Landslide susceptibility mapping using analytical hierarchy process (AHP) in Tehri reservoir rim region, Uttarakhand. *Journal of the Geological Society of India*, *87*(3), 271-286. https://doi.org/10.1007/s12594-016-0395-8

Lai, T., Dragićević, S., & Schmidt, M. (2013). Integration of multicriteria evaluation and cellular automata methods for landslide simulation modelling. *Geomatics, Natural Hazards and Risk*, *4*(4), 355-375. https://doi.org/10.1080/19475705.2012.746243

Lee, S., & Min, K. (2001). Statistical analysis of landslide susceptibility at Yongin, Korea. Environmental Geology, 40(9), 1095-1113. https://doi.org/10.1007/s002540100310

Lee, C. F., Li, J., Xu, Z. W., & Dai, F. C. (2001). Assessment of landslide susceptibility on the natural terrain of Lantau island, Hong Kong. *Environmental Geology*, *40*(3), 381-391. https://doi.org/10.1007/s002540000163

Lee, S., & Pradhan, B. (2006). Landslide hazard mapping at Selangor, Malaysia using frequency ratio and logistic regression models. *Landslides*, *4*(1), 33-41. https://doi.org/10.1007/s10346-006-0047-y

Lin, M., & Tung, C. (2004). A GIS-based potential analysis of the landslides induced by the CHI-CHI earthquake. *Engineering Geology*, *71*(1-2), 63-77. https://doi.org/10.1016/s0013-7952(03)00126-1

McMaster, R. (1997). In memoriam: George F. Jenks (1916-1996). *Cartography and Geographic Information Systems*, *24*(1), 56-59. https://doi.org/10.1559/152304097782438764

MoHA (2017). Nepal Disaster Report, 2017: The Road to Sendai. 2018, Ministry of Home Affairs: Kathmandu

Mondal, S., & Maiti, R. (2013). Integrating the analytical hierarchy process (AHP) and the frequency ratio (FR) model in landslide susceptibility mapping of shiv-khola watershed, Darjeeling Himalaya. *International Journal of Disaster Risk Science*, *4*(4), 200-212. https://doi.org/10.1007/s13753-013-0021-y

Nayak. J. (2010) .Landslide risk assessment along a major road corridor based on historical landslides inventory and traffic analysis. Retrieved on March 5, 2023, from https://library.itc.utwente.nl/papers_2010/msc/aes/nayak.pdf

TckTckTck. (n.d.). Kakani, Bagmati, NP climate zone, monthly averages, historical weather data. Retrieved from https://tcktcktck.org/nepal/bagmati/kakani (Accessed on January 5, 2023).

TckTckTck. (n.d.). *Dhunche, Bagmati, NP climate zone, monthly averages, historical weather data*. Retrieved from https://tcktcktck.org/nepal/bagmati/dhunche ((Accessed on January 5, 2023).

AmeriGEOSS. (2019). Nepal Road Network (Main Roads). AmeriGEOSS. Retrieved from https://data.amerigeoss.org/dataset/nepal-road-network-main-roads (Accessed on January 11, 2023).

Oh, H., & Lee, S. (2010). Cross-application used to validate landslide susceptibility maps using a probabilistic model from Korea. *Environmental Earth Sciences*, *64*(2), 395-409. https://doi.org/10.1007/s12665-010-0864-0

Panchal, S., & Shrivastava, A. K. (2022). Landslide hazard assessment using analytic hierarchy process (AHP): A case study of national highway 5 in India. *Ain Shams Engineering Journal*, *13*(3), 101626. https://doi.org/10.1016/j.asej.2021.10.021

Pardeshi, S. D., Autade, S. E., & Pardeshi, S. S. (2013). Landslide hazard assessment: Recent trends and techniques. *SpringerPlus*, *2*(1). https://doi.org/10.1186/2193-1801-2-523

Park, S., Choi, C., Kim, B., & Kim, J. (2012). Landslide susceptibility mapping using frequency ratio, analytic hierarchy process, logistic regression, and artificial neural network methods at the Inje area, Korea. *Environmental Earth Sciences*, *68*(5), 1443-1464. https://doi.org/10.1007/s12665-012-1842-5

Pathak. D. (2016). REMOTE SENSING AND GIS APPLICATION IN LANDSLIDE RISK ASSESSMENT AND MANAGEMENT. *Nepalese Journal on Geoinformatics*.

Petley, D. (2012) Global Patterns of Loss of Life from Landslides. Geology, 40, 927-

930. https://doi.org/10.1130/G33217.1

Pokharel, B., & Thapa, P. B. (2019). Landslide susceptibility in Rasuwa district of central Nepal after the 2015 Gorkha earthquake. *Journal of Nepal Geological Society*, *59*, 79-88. https://doi.org/10.3126/jngs.v59i0.24992

Pradhan, B., & Lee, S. (2010). Landslide susceptibility assessment and factor effect analysis: Backpropagation artificial neural networks and their comparison with frequency ratio and bivariate logistic regression modelling. *Environmental Modelling & Software*, *25*(6), 747-759. https://doi.org/10.1016/j.envsoft.2009.10.016

Pradhan, B., Lee, S., & Buchroithner, M. F. (2010). Remote sensing and GIS-based landslide susceptibility analysis and its cross-validation in three test areas using a frequency ratio model. *Photogrammetrie - Fernerkundung - Geoinformation*, *2010*(1), 17-32. https://doi.org/10.1127/1432-8364/2010/0037

Quan, H., & Lee, B. (2012). GIS-based landslide susceptibility mapping using analytic hierarchy process and artificial neural network in Jeju (Korea). *KSCE Journal of Civil Engineering*, *16*(7), 1258-1266. https://doi.org/10.1007/s12205-012-1242-0

Regmi, A. D., Yoshida, K., Pourghasemi, H. R., DhitaL, M. R., & Pradhan, B. (2014). Landslide susceptibility mapping along Bhalubang — Shiwapur area of mid-western Nepal using frequency ratio and conditional probability models. *Journal of Mountain Science*, *11*(5), 1266-1285. https://doi.org/10.1007/s11629-013-2847-6

Saaty, T. L. (2008). Decision making with the analytic hierarchy process. International Journal of Services Sciences, 1(1), 83-98. https://doi.org/10.1504/ijssci.2008.017590

Saaty, T.L. (1980). A scaling method for priorities in hierarchical structures. Journal of Mathematical Psychology 15: 234–281.

Sadasivuni, R., O'Hara, C., Nobrega, R., & Dumas, J. (2009). A transportation corridor case study for multi-criteria decision analysis. *American Society for Photogrammetry and Remote Sensing Annual Conference 2009, ASPRS 2009*, *2*,

703–714.

Saha, A. K., Gupta, R. P., & Arora, M. K. (2002). GIS-based landslide hazard zonation in the Bhagirathi (Ganga) Valley, Himalayas. *International Journal of Remote Sensing*, *23*(2), 357-369. https://doi.org/10.1080/01431160010014260

Sentinel-2. (2021). EOS Data Analytics. Retried on March 10, 2023 from https://eos.com/find-satellite/sentinel-2/

Shakya, A. K., Ramola, A., Kandwal, A., & Prakash, R. (2018). Comparison of supervised classification techniques with alos palsar sensor for roorkee region of Uttarakhand, India. *The International Archives of the Photogrammetry, Remote Sensing and Spatial Information Sciences*, *XLII-5*, 693-701. https://doi.org/10.5194/isprs-archives-xlii-5-693-2018

Shano, L., Raghuvanshi, T. K., & Meten, M. (2020). Landslide susceptibility evaluation and hazard zonation techniques – a review. *Geoenvironmental Disasters*, *7*(1). https://doi.org/10.1186/s40677-020-00152-0

Sharma, A., Joshi, V. and Kumar, K. (2011). "Landslide hazard zonation of Gangtok area, Sikkim Himalaya using remote sensing and GIS techniques." Journal of Geomatics, Vol. 5, No. 2, pp. 87-88

Shrestha, A., Ghimire, S., Pokharel, A., Dhami, S., Karki, S., Awasthi, B., & Acharya, T. (2021). Landslide Susceptibility Mapping in Budhi Gandaki River Sub-Basin Using Frequency Ratio and Statistical Information Index. 6.

Sidle, R. C., & Ochiai, H. (2006). Landslides: Processes, prediction, and land use. *Water Resources Monograph*. https://doi.org/10.1029/wm018

Silalahi, F. E., Pamela, Arifianti, Y., & Hidayat, F. (2019). Landslide susceptibility assessment using frequency ratio model in Bogor, West Java, Indonesia. *Geoscience Letters*, *6*(1). https://doi.org/10.1186/s40562-019-0140-4

Sonker, I., Tripathi, J. N., & Swarnim. (2022). Remote sensing and GIS-based landslide susceptibility mapping using frequency ratio method in Sikkim Himalaya. *Quaternary Science Advances*, *8*,

100067. https://doi.org/10.1016/j.qsa.2022.100067

Thapa, D., & Bhandari, B. P. (2019). GIS-based frequency ratio method for identification of potential landslide susceptible area in the Siwalik zone of chatara-barahakshetra section, Nepal. *Open Journal of Geology*, *09*(12), 873-896. https://doi.org/10.4236/ojg.2019.912096

Timilsina, M., & Dahal, R. K. (2013). Landslide hazard in Mugling Road. International Journal of Landslide and Environment, 1(1), 105–106.

Tyagi, A., Kamal Tiwari, R., & James, N. (2022). A review on spatial, temporal and magnitude prediction of landslide hazard. *Journal of Asian Earth Sciences: X*, *7*, 100099. https://doi.org/10.1016/j.jaesx.2022.100099

Veerappan, R., Negi, A., & Siddan, A. (2017). Landslide susceptibility mapping and comparison using frequency ratio and analytical hierarchy process in part of NH-58, Uttarakhand, India. *Advancing Culture of Living with Landslides*, 1081-1091. https://doi.org/10.1007/978-3-319-53498-5_123

WorldClim. (2021). WorldClim - HIstorical Climate Data. Retrieved September 15, 2021, from https://www.worldclim.org/data/worldclim21.htmlWIECZOREK, G. F. (1984). Preparing a detailed landslide-inventory map for hazard evaluation and reduction. *Environmental & Engineering Geoscience*, *xxi*(3), 337-342. https://doi.org/10.2113/gseegeosci.xxi.3.337

Xu, C., F. Dai, X. Xu, and Y. H. Lee. 2012. “GIS-based Support Vector Machine Modeling of Earthquake-triggered Landslide Susceptibility in the Jianjiang River Watershed, China.” Geomorphology 145–146: 70–80. doi:10.1016/j. geomorph.2011.12.040.

Xu, C. (2015). Preparation of earthquake-triggered landslide inventory maps using remote sensing and GIS technologies: Principles and case studies. *Geoscience Frontiers*, *6*(6), 825-836. https://doi.org/10.1016/j.gsf.2014.03.004

Yalcin, A. (2008). GIS-based landslide susceptibility mapping using analytical hierarchy process and bivariate statistics in Ardesen (Turkey): Comparisons of results and

confirmations. CATENA, 72(1), 1-12. https://doi.org/10.1016/j.catena.2007.01.003

Yalcin, A., & Bulut, F. (2006). Landslide susceptibility mapping using GIS and digital photogrammetric techniques: A case study from Ardesen (NE-Turkey). *Natural Hazards*, *41*(1), 201-226. https://doi.org/10.1007/s11069-006-9030-0

Yalcin, A., Reis, S., Aydinoglu, A., & Yomralioglu, T. (2011). A GIS-based comparative study of frequency ratio, analytical hierarchy process, bivariate statistics and logistics regression methods for landslide susceptibility mapping in Trabzon, NE Turkey. *CATENA*, *85*(3), 274-287. https://doi.org/10.1016/j.catena.2011.01.014

Yang, I. T., Acharya, T. D., & Lee, D. H. (2016). Landslide susceptibility mapping for 2015 earthquake region of Sindhupalchowk, Nepal using frequency ratio. *Journal of the Korean Society of Surveying, Geodesy, Photogrammetry and Cartography*, *34*(4), 443-451. https://doi.org/10.7848/ksgpc.2016.34.4.443

Yoon, K., & Hwang, C. (1995). Multiple attribute decision making. https://doi.org/10.4135/9781412985161

Annex

Annex-1: Landslide presence points

S.N	Longitude	Latitude	Elevation(m)	S.N	Longitude	Latidude	Elevation (m)
1	85.22867	27.79073	1316	110	85.28251	28.12137	1545
2	85.23431	27.79255	1574	111	85.27974	28.12224	1685
3	85.20628	28.02915	1185	112	85.28696	28.10713	2000
4	85.20464	28.03145	1159	113	85.30319	28.12229	1550
5	85.23445	27.99594	1411	114	85.30706	28.12383	1986
6	85.23171	27.99982	1651	115	85.30652	28.12567	2002
7	85.22078	28.0627	1710	116	85.30563	28.12606	1932
8	85.26493	27.777	1315	117	85.30598	28.12668	1946
9	85.20929	27.82015	1598	118	85.27662	28.11107	1262
10	85.23539	27.82755	1842	119	85.22739	28.0908	1331
11	85.16625	27.95572	628	120	85.23169	28.09011	1079
12	85.21406	28.01251	1918	121	85.19885	28.05887	1533
13	85.20673	27.99962	1576	122	85.19292	28.03875	833
14	85.2598	27.77419	1300	123	85.19581	28.03609	837
15	85.2131	28.01367	1947	124	85.1928	28.03541	806
16	85.26102	27.80729	1757	125	85.19225	28.02614	772
17	85.24373	27.81871	1852	126	85.18781	28.02742	801
18	85.24393	27.81889	1845	127	85.18961	28.02498	769
19	85.23252	27.82516	1800	128	85.18443	28.02423	776
20	85.22674	27.81734	1761	129	85.17921	28.01413	774
21	85.22536	27.8203	1734	130	85.18064	28.01345	764
22	85.22355	27.8189	1716	131	85.1812	28.01231	756
23	85.2115	27.81759	1584	132	85.18134	28.01143	748
24	85.21191	27.81728	1591	133	85.18536	28.0122	719
25	85.21148	27.81832	1583	134	85.18589	28.01208	751
26	85.20939	27.82087	1560	135	85.18773	28.01136	884
27	85.18086	27.83008	1198	136	85.18562	28.00889	747
28	85.17305	27.83522	1058	137	85.18203	28.00916	726
29	85.17218	27.83716	1044	138	85.18238	28.0076	728
30	85.13859	27.86364	548	139	85.18665	28.00703	758
31	85.23919	27.76675	1279	140	85.18922	28.00571	779
32	85.21074	27.81562	1669	141	85.19103	28.00473	881
33	85.23901	27.77533	1127	142	85.18318	28.0037	699
34	85.23931	27.77527	1126	143	85.18325	27.99994	744
35	85.24177	27.77605	1148	144	85.18389	27.99909	715
36	85.24258	27.77657	1163	145	85.18649	27.99823	672
37	85.24718	27.77778	1161	146	85.18657	27.99782	672
38	85.25008	27.7776	1170	147	85.18822	27.99758	770
39	85.25067	27.77986	1182	148	85.18707	28.0023	704
40	85.2618	27.7838	1369	149	85.188	28.00038	747
41	85.27174	27.78729	1411	150	85.1812	27.99349	740

42	85.27783	27.79357	1602	151	85.18098	27.9943	785
43	85.27689	27.79369	1630	152	85.18315	27.9894	656
44	85.27557	27.79338	1618	153	85.17929	27.98874	702
45	85.26838	27.79164	1635	154	85.17886	27.98785	735
46	85.26735	27.79116	1638	155	85.21158	28.01585	1974
47	85.26938	27.7978	1669	156	85.21784	28.01789	2037
48	85.26943	27.79803	1666	157	85.22389	28.02631	2094
49	85.26982	27.79807	1691	158	85.13712	27.83405	1443
50	85.27026	27.79882	1691	159	85.1412	27.82603	1524
51	85.27449	27.80441	1743	160	85.14529	27.82152	1554
52	85.21396	27.80369	1592	161	85.14453	27.81941	1584
53	85.10686	27.85798	496	162	85.14509	27.81716	1630
54	85.22912	27.79213	1388	163	85.15105	27.81132	1698
55	85.22456	27.8022	1706	164	85.15495	27.81026	1706
56	85.25127	27.79671	1322	165	85.22691	27.80034	1685
57	85.18194	27.95196	1020	166	85.22681	27.8005	1691
58	85.2057	27.98315	1040	167	85.223	27.80266	1687
59	85.21592	27.99743	1350	168	85.21145	27.80507	1725
60	85.22868	27.79209	1371	169	85.19279	27.81913	1985
61	85.23373	27.99265	1282	170	85.19446	27.80679	1823
62	85.23401	27.99767	1519	171	85.18179	27.81541	1618
63	85.26068	27.80806	1808	172	85.18844	27.81816	1836
64	85.25812	27.80985	1813	173	85.21366	27.99086	1116
65	85.23239	27.99682	1493	174	85.20721	27.81096	1926
66	85.18707	27.97911	795	175	85.21317	28.08105	1315
67	85.18806	27.98256	846	176	85.14812	27.87638	545
68	85.23518	27.82906	1782	177	85.18281	28.0013	750
69	85.23466	27.82559	1860	178	85.17225	27.99589	1134
70	85.23219	27.82129	1780	179	85.22713	27.79514	1437
71	85.23174	27.81943	1775	180	85.12563	27.82564	1584
72	85.23183	27.81889	1782	181	85.21165	27.99039	1207
73	85.22974	27.81828	1760	182	85.25091	28.09946	1747
74	85.21591	27.81225	1668	183	85.26936	28.10563	1319
75	85.2137	27.81278	1636	184	85.26071	28.10198	1484
76	85.20745	27.81458	1776	185	85.20069	28.05145	1074
77	85.2115	27.81935	1574	186	85.2288	28.09895	1817
78	85.21067	27.82006	1584	187	85.20971	28.06479	1160
79	85.2093	27.82029	1588	188	85.19666	28.04106	859
80	85.19341	27.83376	1317	189	85.1076	27.84313	1002
81	85.19108	27.83225	1286	190	85.19084	28.01558	985
82	85.18668	27.83447	1248	191	85.10348	27.83992	1154
83	85.16971	27.83128	1106	192	85.10654	27.83997	1122
84	85.16948	27.83162	1118	193	85.12311	27.82477	1582
85	85.16909	27.83893	1021	194	85.12549	27.83246	1459
86	85.14465	27.8652	548	195	85.13159	27.83236	1419
87	85.15669	27.8305	928	196	85.21515	27.99376	1196

88	85.13129	27.86041	520	197	85.21574	27.99446	1206
89	85.1261	27.86345	593	198	85.25176	28.01978	1759
90	85.16399	27.9505	591	199	85.1237	27.83195	1496
91	85.164	27.95209	592	200	85.2534	28.02182	1725
92	85.16151	27.9545	601	201	85.1953	28.04614	1058
93	85.17567	27.96408	617	202	85.22993	27.97881	982
94	85.18757	27.98024	812	203	85.22565	27.98296	1122
95	85.1879	27.98241	840	204	85.16431	27.99292	1010
96	85.1906	27.9864	923	205	85.16479	27.99272	1027
97	85.19629	27.98329	1003	206	85.16592	27.99315	1122
98	85.22015	28.00544	1800	207	85.13583	27.93754	822
99	85.21237	28.01398	1946	208	85.17512	27.99431	997
100	85.27828	28.11215	1252	209	85.22308	27.79024	1428
101	85.27682	28.11409	1346	210	85.12382	27.93696	666
102	85.27772	28.1132	1291	211	85.22413	27.79137	1445
103	85.26192	28.11915	2159	212	85.2472	27.77525	1156
104	85.26607	28.12355	2057	213	85.2466	27.77848	1174
105	85.26974	28.12098	1853	214	85.24581	27.77901	1182
106	85.26743	28.12462	2084	215	85.16831	27.80755	1828
107	85.26593	28.1186	1937	216	85.19086	27.95323	1120
108	85.27611	28.12611	2009	217	85.2438	27.77588	1143
109	85.28249	28.11722	1306	218	85.18176	28.00141	801

Annex-2: Images from field survey